Synthesis of Titanium Dioxide /Reduced Graphene Oxide Nanocomposite using Peel Extracts of *Citrus Aurantium* and *Musa Acum*inata for Photocatalytic Degradation of Methylene Blue from Wastewater

By

Mulugeta Hirko Olana

A Thesis Submitted to Department of Applied Chemistry

School of Applied Natural Science

In Partial Fulfillment of the Requirement for the Degree of Masters of Science in Chemistry (Physical Chemistry)

Office of Graduate Studies

Adama Science and Technology University

December, 2020

Adama, Ethiopia

Synthesis of Titanium Dioxide/ Reduced Graphene Oxide Nanocomposite using Peel Extracts of *Citrus aurantium* and *Musa acuminata* for Photocatalytic Degradation of Methylene Blue from Wastewater

By

Mulugeta Hirko Olana

Major advisor: Bedasa Abdisa (PhD)

Co-advisor: Fedlu Kedir (PhD)

A Thesis Submitted to Department of Applied Chemistry

School of Applied Natural Science

Presented in Partial Fulfillment of the Requirement for the Degree of Masters of Science in Chemistry (Physical Chemistry)

Office of Graduate Studies

Adama Science and Technology University

December, 2020

Adama, Ethiopia

APPROVAL SHEETE

We, the undersigned, members of the Board of Examiners of the final open defense by Mulugeta Hirko Olana entitled“ Synthesis of Titanium Dioxide/ Reduced Graphene Oxide Nanocomposite using Waste Peel Extracts of *Citrus aurantium* and *Musa acuminata* for Photocatalytic degradation of Methylene Blue from Wastewater” have read and evaluated his thesis and examined the candidate. This is, therefore, to certify that the thesis has been accepted in partial fulfillment for the requirement of the Degree, Master of Science in Applied Chemistry (Physical Chemistry).

Mulugeta Hirko	_____	_____
Name of Student	Signature	Date
Bedasa Abdisa (PhD)	_____	_____
Major Advisor	Signature	Date
Fedlu Kedir (PhD)	_____	_____
Co-advisor	Signature	Date
_____	_____	_____
Chairperson	Signature	Date
_____	_____	_____
Internal Examiner	Signature	Date
_____	_____	_____
External Examiner	Signature	Date
_____	_____	_____
Department Head	Signature	Date
_____	_____	_____
School Dean	Signature	Date
_____	_____	_____
Postgraduate Dean	Signature	Date

DECLARATION OF STUDENT AND ADVISOR

I hereby declare that this MSc Thesis is my original work and has not been presented for a degree in any other university, and all sources of material used for this thesis/ dissertation have been duly acknowledged.

Name: _____

Signature: _____

This MSc has been submitted for examination with my approval as thesis advisor.

Name: _____

Signature: _____

Name: _____

Signature: _____

Date of submission_____

ADVISOR'S APPROVAL SHEET

To: Applied Chemistry Department

Subject: Thesis Submission

This is to certify that the thesis entitled ''Synthesis of Titanium Dioxide /Reduced Graphene Oxide Nanocomposite using Peel Extracts of *Citrus Aurantium* and *Musa Acum*inata for Photocatalytic Degradation of Methylene Blue from Wastewater'' submitted in partial fulfillment of the requirements for the degree of Master's in Physical chemistry, the Graduate program of the department of Applied Chemistry, and has been carried out by Mulugeta Hirko Olana Id. No PGR/18158/11, under our supervision. Therefore, we recommend that the student has fulfilled the requirements and hence hereby he can submit the thesis to the department.

_____	_____	_____
Name of major Advisor	Signature	Date
_____	_____	_____
Name of Co-advisor	Signature	Date

ACKNOWLEDGMENT

I would like to express my gratitude and appreciation as well as deep sense of dedication to my major advisor Dr. Bedasa Abdisa and co-advisor Dr. Fedlu Kedir for theirs enthusiastic encouragements, skillful guidance's, comments, and patiently suggestions during the course of my study.

I also greatly acknowledge and love to express my gratitude to Material Science and Engineering, Chemical Engineering and Applied Biology Departments, for letting me use their laboratory facilities and sample characterizations during my study.

My heartfelt appreciation goes to Mrs. Eneyehu Tilahun and my friends for their cooperation and provides necessary facilities to me during this study and for the completion of this research work.

I honorably express my deepest gratefulness towards my wife Workinesh Fekadu and my Son Segni Mulugeta, who have always supported me technically and morally for the successful accomplishment of my work. Last but not the least, my humble and absolute obeisance to Almighty God who has guided me through all good and bad times.

TABLE OF CONTENTS

LIST OF TABLE

LIST OF FIGURE

LIST OF ABBREVIATION AND ACRONYM

2D	Two dimensional
CA/c	*Citrus aurantium*
CVD	Chemical vapor deposition
D	Crystal size in diameter
DTA	Differential thermal analysis
Eg	Band gap Energy
FT-IR	Fourier transforms infrared
FWHM	Full width at half maximum
GO	Graphene oxide
G-N	Graphene nanoparticles
MA/m	*Musa acuminate*
MB	Methylene blue
NC	Nanocomposite
NPs	Nanoparticles
rGO	Reduced graphene oxide
SEM	Scanning electron microscopy
TGA	Thermal gravimetric analysis
UV –VIS	Ultra violet visible
XRD	X-ray-diffraction

ABSTRACTS

In this research, titanium dioxide and surface modified TiO_2 with reduced graphene oxide (TiO_2/rGO) nanocomposite were synthesized. TiO_2 nanoparticle was synthesized by sol-gel method from titanium tetra butoxide precursor and steam extracts of orange (citrus aurantium) and banana (musa acuminata) peels which were used as reducing, capping and stabilizing agents. GO was synthesized by Tour method using graphite powder with addition of $KMnO_4$ and H_2O_2 strong oxidizing agents in the presence of concentrated H_2SO_4 and H_3PO_4. The surface modified TiO_2/rGO was synthesized from green synthesized TiO_2 and GO by addition of citrus aurantium and musa acuminate extracts by co-precipitation method. The synthesized Titanium dioxide/ reduced graphene oxide nanocomposite and Titanium dioxide were characterized using Fourier transform infrared spectroscopy (FTIR) for functional groups analysis, scanning electron microscopy (SEM) for morphological studies, UV-Vis spectroscopy for optical properties study and X-ray powder(XRD) for the crystal structures analysis. The photocatalytic degradation performances of MB from synthetic waste water were investigated by using TiO_2 and TiO_2/rGO for both extracts. When we compare degradation efficiency of TiO_2 and TiO_2/rGO, TiO_2/rGO (94.28%) nanocomposite was 1.62 times more efficient than TiO_2 (58.2%) nanoparticles within 60 minutes in the presence of halogen lamp. A Photocatalytic activity of TiO_2/rGO nanocomposite was studied at different conditions like catalytic doze, initial concentration of pollutant, pH and reaction time effects. Catalytic dosage, pH and reaction time have positive effect, but initial concentration of pollutant has negative effect on photocatalytic degradation of methylene blue from synthetic waste water.

Key word: *Titanium dioxide nanoparticles, reduced graphene oxide, nanocomposite, photocatalytic degradation, methylene blue*

1. INTRODUCTION

1.1 Background of the Study

A dye is a colored chemical substance that imparts color when applied to a substrate. Which is generally soluble in solvents, and they can be natural or synthetic. The residual dyes from different sources such as textile, pulp paper, pharmaceutical and tannery industries are wide variety of organic pollutants introduced into our natural water resources or wastewater treatment units. One of the main sources with severe polluting problem worldwide is the textile industry and its wastewater containing dyes, 10 – 25% of the textile dyes are lost. During dying process 2-20% are directly discharged as aqueous effluents in different environmental components [1].

The discharge of effluents containing dyes into water is undesirable due to its color, dyes released and the breakdown products of dyes which are toxic, carcinogenic to life mainly because of the presence of carcinogens present such as naphthalene, benzamine and other aromatic compounds. If not treated these remain in the environment for a long period of time (1-3 years). So recycling of treated wastewater should be done [2].

The organic dyes can be separated and eliminated from water by effective and viable treatment at sewage treatments works or on site by trying to remove or degrade. Due to diverse chemical nature of textile effluents, they are difficult to treat by conventional purification procedures. Treatments like chlorination cannot be used as it release mutagenic products even from less harmful dyes [3]. Therefore, these contaminants have to be removed efficiently from the industrial effluent and thus from the environment for the sake of human and environmental well-being. With this in mind, the application of metal oxide nanomaterials for photo-degradation of organic pollutant in wastewater becomes the main research area.

TiO_2 NPs is a good candidate for photo-catalytic degradation of organic pollutant because of its low cost, high photosensitivity, and nontoxic nature. However, the rapid charge carrier recombination and wide band gap of TiO_2 limit its solar energy harvesting for photocatalyst efficiency. One of the best approaches to overcome these issues is coupling TiO_2 NPs with other nanomaterials such as reduced graphene oxide or graphene NPs to construct hetero-structure which can significantly enhance the charge carrier separation by

decreasing its energy band gap of TiO_2. Graphene or reduced graphene oxide NPs is used to trap the electron from conduction band before recombine with holes that generated in valance band [4].

Several chemical synthesis techniques have been used for the synthesis of TiO_2/rGO nanocomposite. However green synthesis process has been accepted as a promising technique to prevail the limitations accompanied with chemical methods [5].

Here in, *citrus aurantium* and *musa acuminata* fruit peel extracts were used as reducing and capping agent for the synthesis of TiO_2/rGO nanocomposite. The stimulant effects are mainly related to the presence of bioactive molecules such as terpenes, oxygenated derivatives, aldehyde (citral), alcohols and esters from citrus *aurantium* and lignin, cellulose, hemicellulose and pectin lignin, cellulose, hemicellulose and pectin compounds from *musa acuminata* [6]. In addition to these the fruit peels contain polyphenols, amino and carboxylic groups that may help as stabilizers, favoring the conversion of metal compounds into specific NPs.

Therefore, in this study TiO_2 nanoparticle was synthesized using peel extracts of orange (*Citrus aurantium*) and banana (*musa acuminata*) and modified with reduced graphene oxide (TiO_2/rGO) for photocatalytic degradation of MB from synthetic wastewater [7].

1.2 Statement of the Problem

Dyes are the major water pollutants that even in small amount easily decolorize surface of water and cause pollution. Some conventional waste treatment methods such as chlorination, coagulation, dual-media filtration and flocculation were used to remove these from wastewater even though they are not effective [8]. Furthermore, these methods also impose carcinogenic chemicals by reacting with dyes. As a result of this new technology, nanotechnology: the designing, synthesis and application of nanomaterials, has emerged for waste water treatment [9].

One of the nanomaterials that widely applicable in the field of energy and environmental remediation is TiO_2 nanoparticles. TiO_2 is low cost, more stable and environmental manageable material oxide. One of the draw backs of using TiO_2 is recombination of holes and electrons that decrease the photocatalytic activity of TiO_2 NPs. As a result, surface modification of TiO_2 nanoparticles by doping with metal or nonmetal elements and

synthesizing composite are the best method to overcome the challenges. Reduced graphene Oxide is one of the best materials used for synthesizing TiO_2/rGO nanocomposite that trap electrons to prevent recombination with holes [10].

Green method is the best method to synthesize TiO_2/rGO nanocomposite due to low cost, environmental friend, and easily manageable routes. Green synthesis of TiO_2/rGO nanocomposite using different plants extracts was reported. But to the best of my knowledge synthesis of TiO_2/rGO using waste fruit peel extracts of *citrus aurantium* and *musa acuminata* by co-precipitation method was not reported. Therefore, in this study the extracts of *citrus aurantium* and *musa acuminata* were used as reducing, stabilizing and capping agents for synthesis of TiO_2/rGO nanocomposite. Furthermore, surface modification of TiO_2 nanoparticles was carried out by using graphene oxide to synthesize TiO_2/reduced graphene oxide nanocomposite by co-precipitation method and used for photocatalytic degradation of methylene blue from synthetic wastewater [11].

1.3 Objectives of the Study

1.3.1 General Objective

The general objective of this research was to synthesize TiO_2/rGO nanocomposite by green method using waste fruit peel extracts of *Citrus aurantium* and *Musa acuminata* and investigate its photocatalytic degradation of methylene blue from synthetic wastewater.

1.3.2 Specific Objectives

The specific objectives of this study were:

- To synthesize, TiO_2 NPs and TiO_2/rGO NC (using waste peel extracts of *citrus aurantium* and *musa acuminata)* as reducing agent and GO by using Tour method;
- To characterize the synthesized GO, TiO_2 NPs and TiO_2/rGO NC using TGA/DTA, UV-Vis, FT-IR, XRD and SEM instruments;
- To evaluate the photocatalytic activity of synthesized TiO_2 NPs and TiO_2/rGO nanocomposite for photocatalytic degradation of MB.
- To evaluate the effect of reaction time, pH, initial concentration of pollutant and catalytic dosage on photocatalytic degradation of MB by TiO_2/rGO NC.

1.4 Significances of Study

This study would provide information about the green synthesis of TiO_2/rGO nanocomposite using *citrus aurantium* and *musa acuminata* extracts by co-precipitation method. Furthermore, the findings of this study would be used as a base by interested researchers for further study in the area.

1.5 Scope of the Study

The research work was limited to green synthesis of TiO_2 /rGO using *citrus aurantium* and *musa acuminate* by co-precipitation method, Characterization of the synthesized nanocomposite using UV-Vis, FTIR, XRD and SEM instruments, and application of TiO_2 NPs, TiO_2/rGO nanocomposite as photocatalytic degradation of MB from synthetic wastewater.

2. LITERATURE REVIEW

2.1 Nanoparticles

Nanoparticles**,** ultrafine unit with dimensions measured in nanometers (nm; 1 nm = 10^{-9} meter). Nanoparticles exist in the natural world and are also created as a result of human activities. Because of their submicroscopic size, they have unique material characteristics, and manufactured nanoparticles may find practical applications in a variety of areas, including medicine, engineering, catalysis, and environmental remediation [12].

In 2008 the International Organization for Standardization (ISO) defined nanoparticles as a discrete nano-object where all three Cartesian dimensions are less than 100 nm. The ISO standard similarly defined two-dimensional nano-objects (i.e., nanodiscs and nanoplates) and one-dimensional nano-objects (i.e., nanofibres and nanotubes). But in 2011 the Commission of the European Union endorsed a more-technical but wider-ranging definition [13]:

Under that definition a nano object needs only one of its characteristic dimensions to be in the range 1–100 nm to be classed as nanoparticles, even if its other dimensions are outside that range. (The lower limit of 1 nm is used because atomic bond lengths are reached at 0.1 nm.) That size range from 1 to 100 nm overlaps considerably with that previously assigned to the field of colloid science from 1 to 1,000 nm which is sometimes alternatively called the mesoscale. Thus, it is not uncommon to find literature that refers to nanoparticles and colloidal particles in equal terms. The difference is essentially semantic for particles below 100 nm in size [14].

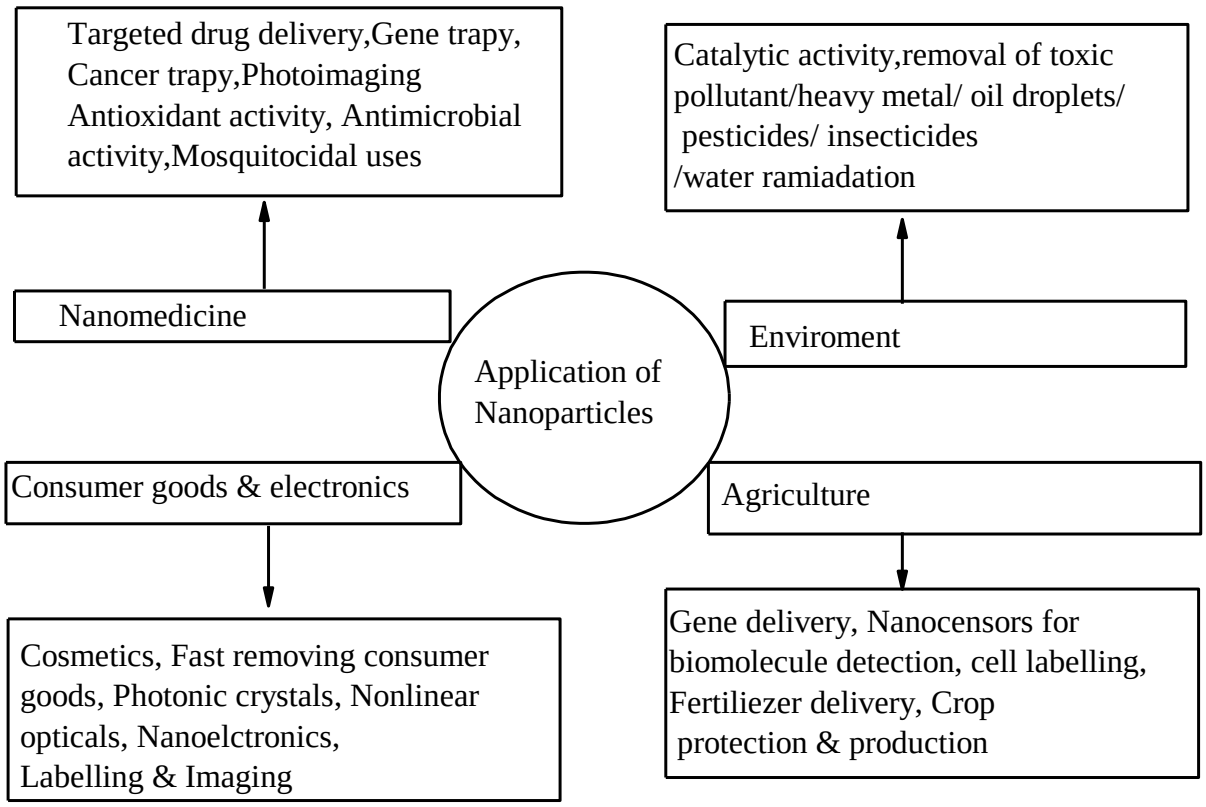

Figure 1.Application of fabricated nanoparticles in cutting-edge areas [14].

2.2 Classification of Nanoparticles

Nanoparticles can be classified into any of various types, according to their size, shape, and material properties. Some classifications distinguish between organic and inorganic nanoparticles; the first group includes dendrimers, liposomes, and polymeric nanoparticles, while the latter includes fullerenes, quantum dots, and gold nanoparticles. Other classifications divide nanoparticles according to whether they are carbon-based, ceramic, semiconducting, or polymeric. In addition, nanoparticles can be classified as hard (e.g., Titania [titanium dioxide], silica [silica dioxide] particles, and fullerenes) or as soft (e.g., liposomes, vesicles, and nanodroplets). The way in which nanoparticles are classified typically depends on their application, such as in diagnosis or therapy versus basic research, or may be related to the way in which they were produced [15].

2.2.1 Carbon-Based Nanoparticles

Fullerenes and carbon nanotubes represent two major classes of carbon-based nanoparticles. Fullerenes contain nanomaterial that is made of globular hollow cage (Figure 2) such as allotropic forms of carbon. They have created noteworthy commercial

interest due to their electrical conductivity, high strength, structure, electron affinity, and versatility. These materials possess arranged pentagonal and hexagonal carbon units, while each carbon is sp^2 hybridized. They are widely synthesized by deposition of carbon precursors especially the atomic carbons, vaporized from graphite by laser or by electric arc on to metal particles. Lately, they have been synthesized via chemical vapor deposition technique. Due to their unique physical, chemical and mechanical characteristics, these materials are not only used in pristine form but also in nanocomposites for many commercial applications such as fillers, efficient gas adsorbents for environmental remediation , and as support medium for different inorganic and organic catalysts [16].

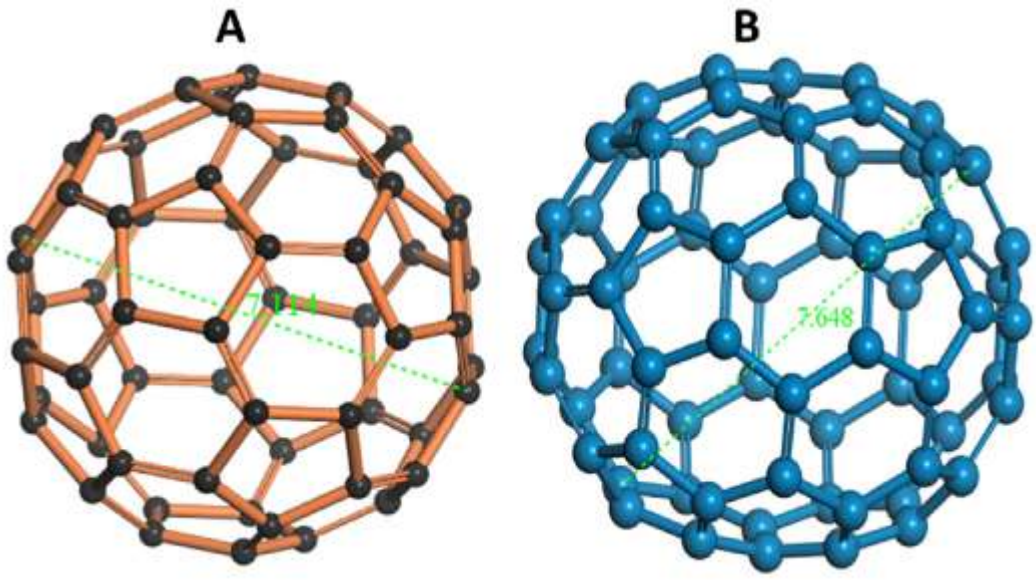

Figure 2 Different form of Fullerenes/buck balls (A) C60and (B) C70 [16].

2.2.2 Metal Nanoparticles

Metal NPs are purely made of the metals precursors. Due to well-known localized surface Plasmon resonance characteristics, these NPs possess unique optoelectrical properties. NPs of the alkali and noble metals i.e. Cu, Ag and Au have a broad absorption band in the visible zone of the electromagnetic solar spectrum. The facet, size and shape controlled synthesis of metal NPs is important in present day cutting-edge materials [17]. Due to their advanced optical properties, metal NPs find applications in many research areas.

2.2.3 Ceramics Nanoparticles

Ceramics NPs are inorganic nonmetallic solids, synthesized via heat and successive cooling. They can be found in amorphous, polycrystalline, dense, porous or hollow forms.

Therefore, these NPs are getting great attention of researchers due to their use in applications such as catalysis, photocatalysis, photodegradation of dyes, and imaging applications. The most commonly used NPs for the design of nanocarriers are Al_2O_3 and TiO_2 [18].

2.2.4 Semiconductor Nanoparticles

Semiconductor materials possess properties between metals and nonmetals and therefore they found various applications in the field of science due to this property. Semiconductor NPs possess wide band gaps and therefore showed significant change in their properties with band gap tuning. Therefore, they are very important materials in photocatalysis, photo optics and electronic devices. As an example, TiO_2 semiconductor NPs is found exceptionally efficient in water splitting applications, due to their suitable band gap and band edge positions [19].

2.2.5 Polymeric Nanoparticles

Polymeric nanoparticles are particles within the size range from 1 to 1000 nm and can be loaded with active compounds entrapped within or surface adsorbed onto the polymeric core. These are normally organic based NPs and in the literature a special term polymer nanoparticles collective used. They are mostly nanospheres or nanocapsules shaped. The former are matrix particles whose overall mass is generally solid and the other molecules are adsorbed at the outer boundary of the spherical surface. In the latter case the solid mass is encapsulated within the particle completely. The polymer NPs are readily functionalize and thus find bundles of applications [20]. The most widely used synthetic polymers are polylactide, polylactide polyglycolide copolymers, polycaprolactones, and polyacrylates. Lactide glycoside copolymer is an extensively explored copolymer. Among the various natural polymers, alginate, albumin, or chitosan have been widely explored [21] .

2.2.6 Lipid-Based Nanoparticles

These NPs contain lipid moieties and effectively using in many biomedical applications. Generally, a lipid NP is characteristically spherical with diameter ranging from 10 to 1000 nm. Like polymeric NPs, lipid NPs possess a solid core made of lipid and a matrix contains soluble lipophilic molecules. Surfactants or emulsifiers stabilized the external core of these

NPs. Lipid nanotechnology is a special field, which focus the designing and synthesis of lipid NPs for various applications such as drug carriers and delivery and RNA release in cancer therapy [22].

2.3 Titanium Dioxide (TiO_2) Nanoparticles

Titanium dioxide (TiO_2), also called titanium (IV) oxide, was initially discovered in 1821 but marketed in 1916 as a white pigment. It is found in nature in three crystallographic forms: rutile, anatase and brookite. Only the anatase and rutile crystalline structures are used commercially, and are found in manufactured products for which the risk of exposure is of interest for toxicological studies. The anatase phase is metastable whereas the rutile phase is thermodynamically stable. For nanoparticles less than 15 nm, the anatase phase becomes the most stable because stability depends on the size of the particles. Nanoparticles have unique properties relative to the large particles, allowing their use in many nanomaterials. For example, TiO_2 nanoparticles are widely used in cosmetics, paints and foodstuffs for their various properties, including colloidal stability, high reflection index and photocatalytic properties. In particular, the very large specific surface area of nanomaterials greatly increases their surface reactivity with biological media [23]. Figure 3 shows the three crystallographic forms of titanium dioxide.

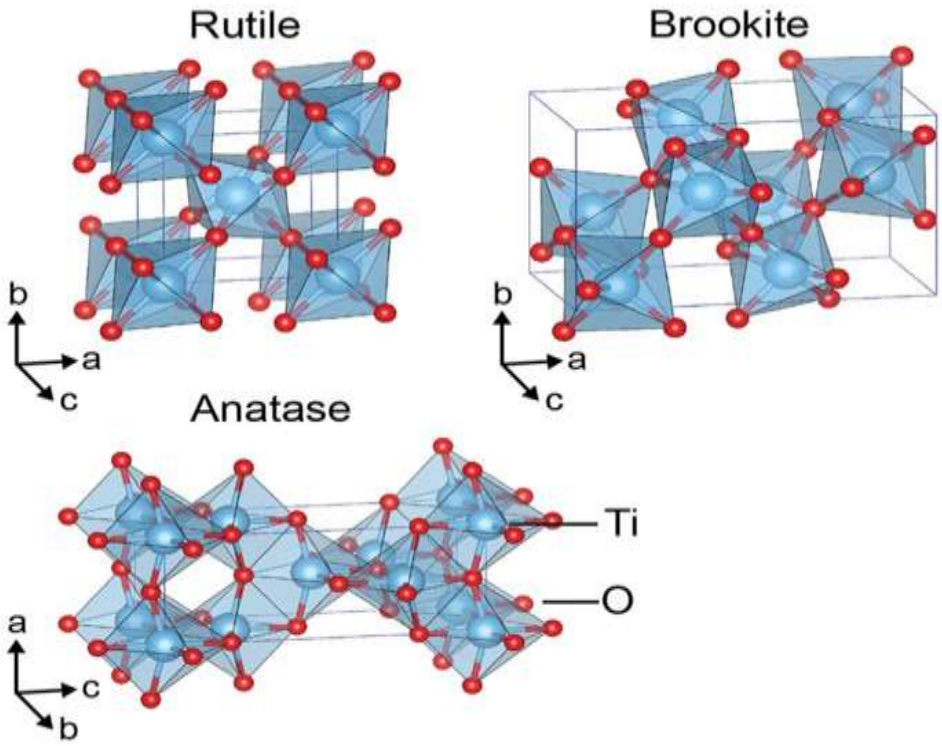

Figure 3. The anatase, rutine and brookite phase Structures of TiO_2 nanoparticle [24]

2.3.1 Synthesis of TiO_2 NPs

There are different methods for the synthesis of nanoparticles and these methods are dividing into two main classes show in Figure 4.

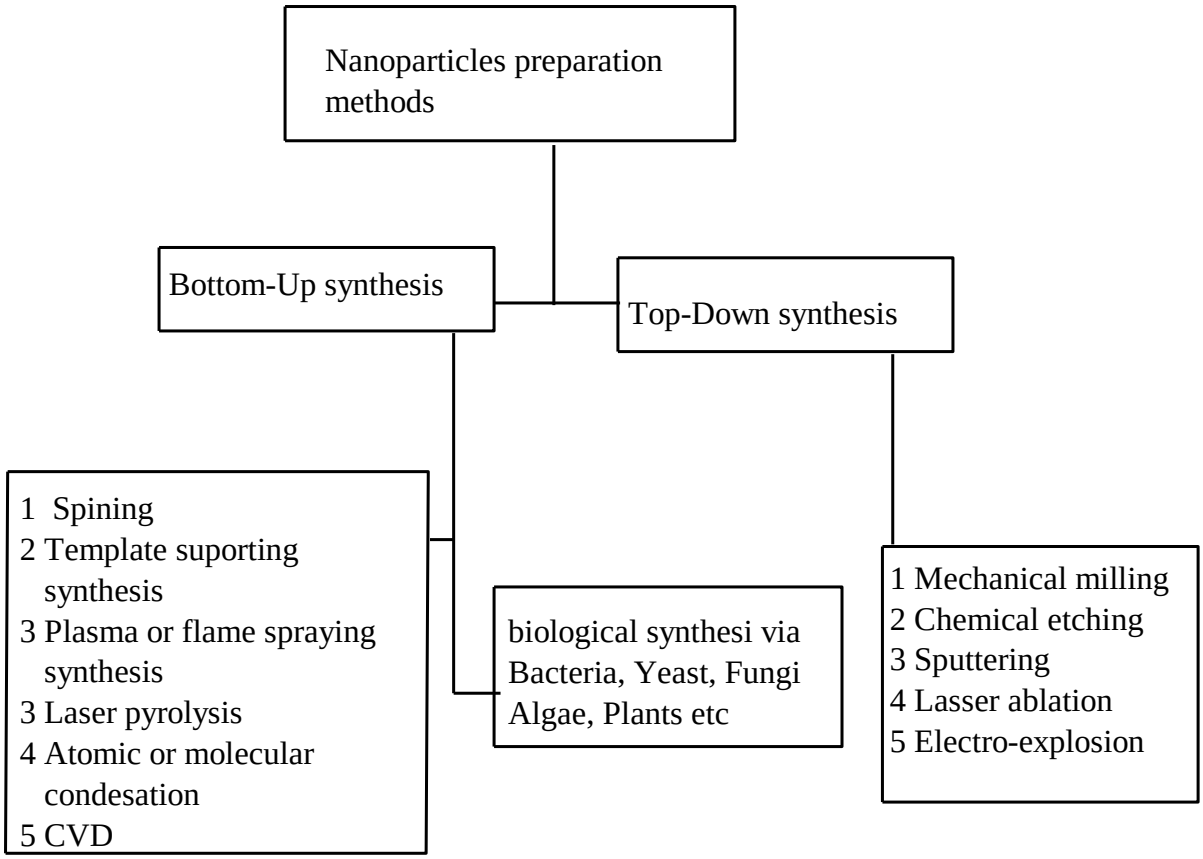

Figure 4 Both Top-down and Bottom-up approach synthesis methods of nanomaterials [15].

In this synthesis, destructive method is used. The larger molecule (bulk material) decomposed into a smaller molecule and then these smaller molecules transform into the nanoparticles. Grinding or milling, physical vapor deposition and other destructive approaches are the example of Top-down synthesis.

Bottom-up synthesis is also known as constructive method. It is the reverse of top-down method. In this method, nanoparticles are formed from relatively simpler substances. Bottom-up method includes Chemical vapor deposition (CVD), Sol–gel, spinning, pyrolysis and biological synthesis [15].

Several techniques are developed day by day for the synthesis of nanoparticles. There are three basic categories of these techniques which are biological methods, physicals method and chemical methods. The best method for synthesis of nanoparticles is the Biological

method due to simplicity, nontoxic and cost effectiveness. The capping and reducing agents are playing important role in the synthesis of nanoparticles. Hazardous and highly toxic chemicals are used in the chemical and physical method of nanoparticles synthesis which are responsible for defect in the environment. The reducing or capping agent used in chemical and physical methods is expensive. Biologically developed chemicals are used in biological method which is not harmful for our environment. Thus the most preferable process for synthesis of nanoparticles is biological method [25].

2.3.1.1 Biological Synthesis of Nanoparticles

Biological synthesis involves the synthesis of nanoparticles by using plant extract and microorganisms such as bacteria and fungi.

Phytonanotechnology has shown a new field for the synthesis of nanoparticles which is eco-friendly, simple, cost effective. Scalability, biocompatibility and synthesis of nanoparticles via universal solvent (water) as reducing agents are advantages of phytonanotechnology. Phytonanotechnology use plants for synthesis of nanoparticles. Nanoparticles are synthesizes using different part of plant such as root, fruit, stem, seed and leaf. The exact mechanism for synthesis of nanoparticles using plant remains to be elucidated. It has been illustrated that organic acid, proteins vitamins and secondary metabolites such as alkaloids, flavonoids, terpenoids, polysaccharides and heterocyclic compound are responsible for synthesis of various types' nanoparticles [26].

Microorganism is considered nanofactories that hold wide potential as cost effective tool, eco-friendly, avoid toxic and harsh chemicals and energy demand for the synthesis of nanoparticles. Various reductase enzymes present in the microorganism due to which microorganism have ability to accumulate and detoxify heavy metals. These reductase enzymes play vital role in reduction of metal salt into the nanoparticles. Over past few year, various microorganism such yeast, fungi and bacteria. Proteins, reducing cofactor, metal resistant gene, enzyme and organic material play important role in synthesis of nanoparticles as reducing and capping agent [27].

Advantages of green or biological synthesize over physical and chemical methods rare: Energy Efficient, low cost production, fewer accident, safe product and economical, lesser waste therefore it is also called as environmental friendly, competitive advantages,

protect human health and communities, use in pharmaceutical industry and other biomedical application [28].

a. Synthesis of TiO_2 Nanoparticles using Bacteria

The first reports using microorganisms, bacteria were utilized to synthesize nanoparticles earlier. Due to the mild conditions, high yield and easy purification, bacteria become the most widely studied microorganism, with the title of "the factory of nanomaterials". Bacteria have been most extensively researched for synthesis of TiO_2 nanoparticles because of ease of manipulation. Bacteria produce inorganic nanomaterials like TiO_2 either intracellularly or extracellularly often in nanoscale dimensions with exquisite morphology. Synthesis using bio-organisms is compatible with the green chemistry principles: the bio-organism is eco-friendly as are the reducing agent employed and the capping agent of the reaction [29].

b. Synthesis of TiO_2 Nanoparticles using Fungi

Fungi can be used as excellent source of various extracellular enzymes which influences TiO_2 nanoparticles synthesis. It was found that fungi are almost ideal biocatalysts for TiO_2 NPs biosynthesis, in contrast to bacteria, as they are well known for producing greater amounts of biologically active substances that make the fungus more appropriate for large scale production. Furthermore, fungal biomass can resist flow pressure, agitation and harsh conditions in chambers such as bioreactors. They also exude extracellular reductive proteins which can be used in subsequent process steps. Moreover, the cell is deprived of unessential cellular components since NPs are accelerated outside the cell and can be immediately used in manifold ways without pretreatment [30].

c. Synthesis of TiO_2 Nanoparticles using Algae

Available functional groups and enzymes in the algal cell walls act as reducing agents, as a consequence of which reduction and fabrication of TiO_2 metal oxide nanoparticles occur at ambient conditions. Algae are a rich source of biomolecules and frequently used for the extracellular synthesis of nanoparticles. Algae may produce TiO_2 nanoparticles from metal salts by extracellular or intracellular pathways involving biochemicals or enzymes present in them. However, enzymes and reducing substances are known to be the main constituents of microorganisms and for the production of metal nanoparticles from metal salts [31].

d. Synthesis of TiO_2 NPs Nanoparticles using Plant Extracts

Researchers reported that the rate of synthesis of nanoparticles is very high when they use plant extracts instead of microorganisms for biosynthesis of metal nanoparticles, which is a more rapid and reproducible process. The nature of plant extract affects the kind of nanoparticles synthesized in a highly critical manner with the source of plant extract being the most vital factor affecting the morphology of synthesized nanoparticles due to different phytochemical composition of plants used. Figure 5 shows the plant mediated synthesis of nanoparticles [32].

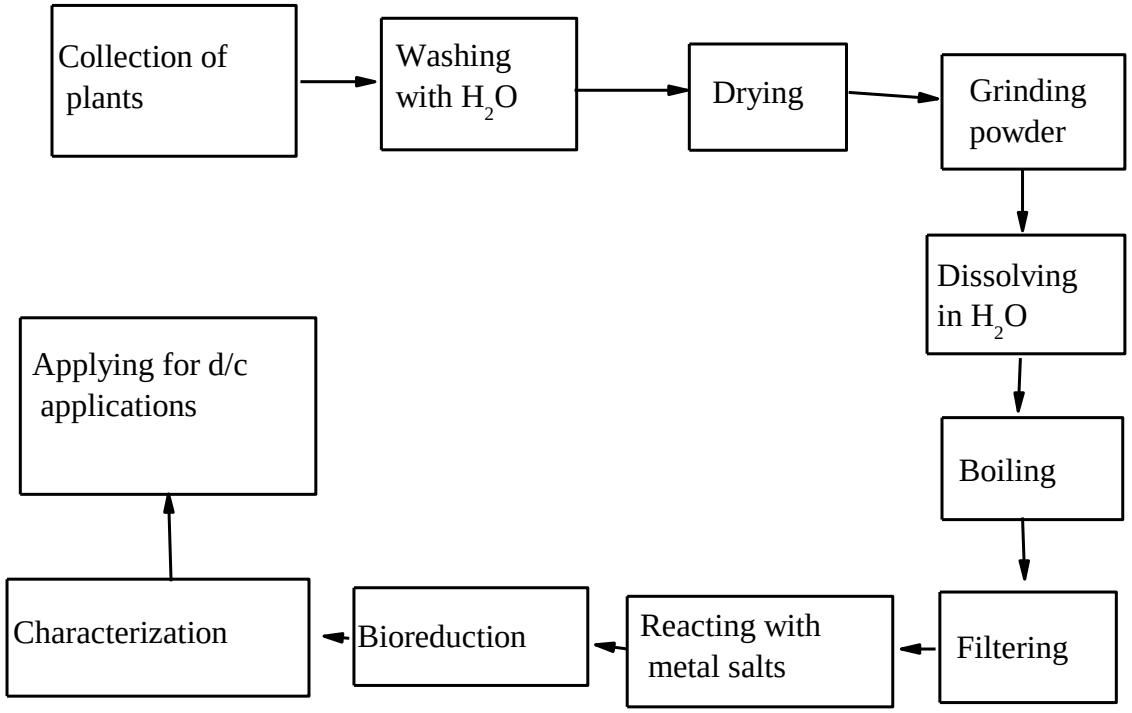

Figure 5. Nanoparticles synthetic pathway using plant extracts [32].

Various parts of green plants can be used for synthesis of TiO_2 and for other metal nanoparticles including leaves, stems, roots and seeds. It has been reported that the photochemical, primary and secondary metabolites are well known as natural resources that are responsible for metal salt reductions. The green synthesized TiO_2 NPs shows the best photocatalyst activity due to its long thermodynamic stability and strong oxidizing power [33].

2.3.2 Photocatalytic Application of TiO_2 Nanoparticles

The word photocatalysis is composed of two parts: Photo and catalysis. The prefix photo is defined as "light". Catalysis is the process where a substance participates in modifying the rate of a chemical transformation of the reactants without being altered in the end. The substance is known as catalyst which increases the rate of a reaction by reducing the activation energy. Hence photocatalysis is a reaction which uses light to activate a substance which modifies the rate of a chemical reaction without being involved itself. Photocatalytic oxidation, also known as heterogeneous photocatalysis, has been used since the mid-1970s to decontaminate water from harmful microorganisms [34].

The most commonly used and researched semiconductor photocatalyst, TiO_2, is used as the substrate, and H_2O and O_2 are used as adsorbates. TiO_2 NPs photocatalyst has the following phases: TiO_2 absorbs Ultraviolet radiation from sunlight; generation of negative - electron (e^-) and positive - hole (h^+) pair; Water splitting reaction occurred and finally organic pollutant is split up to harmless products. The primary criteria for an efficient semiconductor photocatalyst are that the redox potential of the charge couple, i.e. e/h^+, lies within the band gap domain of the photocatalyst. A molecular description of a general photocatalytic reaction process is given by Equations from 1- 8 [35].

Absorption of efficient photons ($hv > {}_{Eg} = 3.2eV$) by TiO_2.

$$TiO_2 + hv \rightarrow TiO_2 (h^+_{vb} + e^-_{cb}) \quad \text{.....1}$$

Oxygen ion sorption (first step of oxygen reduction; oxygen's oxidation passes from 0 to -1/2)

$$O_2 \text{ ads} + e^- \rightarrow O_2^{\cdot} \quad \text{..... 2}$$

Neutralization of ^-OH groups by photo holes which produces OH° radicals.

$$(H_2O \leftrightarrow H^+ + {}^-OH) \text{ ads} + h^+ vb \rightarrow H^+ + {}^-OH \quad \text{.....3}$$

Neutralization of $O_2^{\cdot -}$ by photons

$$O_2^{\cdot -} + H^+ \rightarrow HO_2^{\circ} \quad \text{..... 4}$$

Transient H_2O_2 formation and dismutation of oxygen

$2H_2O° \rightarrow \quad H_2O_2 + O_2$ ……..……..……..... 5

Decomposition of H_2O_2 and second reduction of oxygen

$H_2O_2 + e^- \rightarrow OH° + {}^{\cdot}OH$ ……..…..... 6

Oxidation of the organic reactant / dyes via successive attacks by OH° radicals

$R/MB + {}^{\cdot}OH \rightarrow R^{\cdot} + H_2O$……7

Direct oxidation by reaction with holes

$R + h^+ \rightarrow R^{\cdot +} \rightarrow CO_2 + H_2O +$ others ……...8

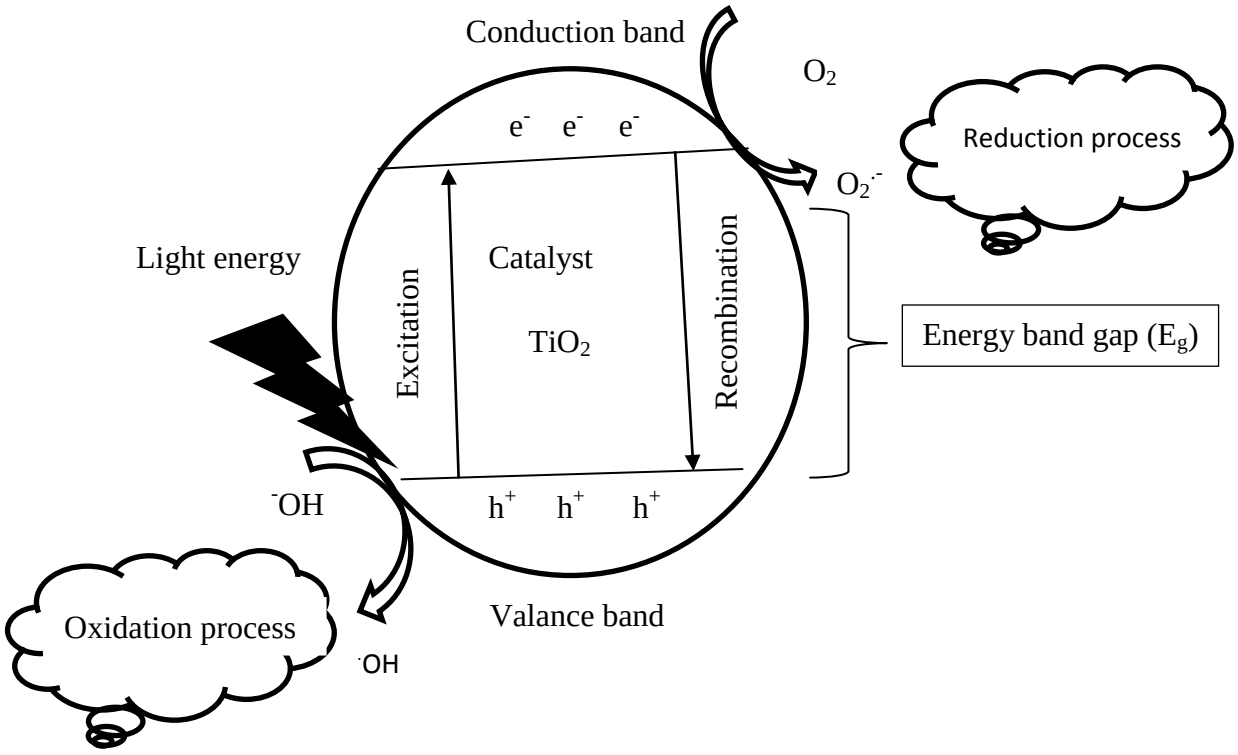

Figure 6. Schematic representation of semiconductor photocatalytic mechanism [36].

a. TiO_2 Nanoparticles in Wastewater Treatment

Among the various metal oxide nanoparticles, titanium dioxide nanoparticles have wide applications in water purification due to their potential oxidation strength, high photo stability and non-toxicity. In particular, dye degradation is almost essential for wastewater treatment due to its toxicity. Titanium dioxide exists in three main polymorphs i.e. Anatase,

Rutile and Brookite. Among these, Anatase TiO_2 exhibits high photocatalytic activity due to high absorption capacity towards organic, molecular oxygen and low rate of recombination of electron hole pairs. Due to antifogging effect of TiO_2 NPs, it removes bacteria and different harmful organic materials from water [37].

Water treatment by TiO_2 Photocatalysis has some benefits compared to conventional water treatment methods. The most important is that it can completely mineralize almost any chemicals and biological compounds, instead of just transferring them to another state. Moreover, the oxidation potential of TiO_2 photocatalysis is higher than normal UV and H_2O_2 treatments. Other beneficial properties making TiO_2 a feasible candidate to waste water treatment is that it is effective at ambient temperatures and pressures and therefore in principle allow for low operating costs. Textile and paper industries discharge huge amount of pollutants and carcinogenic dye effluents into the environment without any pre-treatment. All these dye pollutants are chemically stable which makes them hard to be degraded. Recently, TiO_2 nanoparticles photocatalytic degradation has emerged as an alternative solution to solve such problem. This is owing to its capability in decolorizing and degrading the dyes to other degradation products which are not harmful to different parts of the environment like water bodies [38].

b. TiO_2 Nanoparticles s for Organic Matter Removal

Recently, the application of TiO_2 as a photocatalyst on the removal of organic, inorganic and other pollutants has attracted much researcher's effort. Previous research was reported that chlorinated pesticides could be degraded and mineralized through the photocatalytic reaction of TiO_2 under UV light. In the presence of TiO_2 at 300 nm irradiation, photocatalytic degradation of dicamba herbicide could be increased by 3 times compared with those without TiO_2 addition. The reaction rate is also somewhat related to pH change; neutral medium is more suitable than acidic or alkaline environment as the increase of hydroxide ions and charges repulsion [39].

c. TiO_2 Nanoparticles in Water Splitting

Modern society has been searching for a new form of energy that is clean renewable, cheap and a viable alternative to fossil fuels due to the drastic depletion of fossil fuels by their effective consumption and the serious environmental problems accompanying their combustion. In the development of new energy sources, hydrogen is one of the most

attractive fuels for the 21st century. Hydrogen is considered as an ideal fuel for the future and it can be produced from clean and renewable energy sources and, thus, its life cycle is clean and renewable. Renewable hydrogen production is not popular yet because the cost is still high. However Photovoltaic water electrolysis may become more competitive as the cost continues to decrease with the technology advancements. Photoelectrolysis uses sunlight to directly decompose water into hydrogen and oxygen. The photocatalytic splitting of water into hydrogen and oxygen using solar energy is a challenging research topic which has received much attention in recent years for its potential to provide clean and renewable H_2 as energy resources [40].

2.3.3 Factors Affecting Photocatalytic Applications of TiO_2 Nanoparticles

In photocatalytic degradation the followings are operating parameters which affect the process of photocatalysis: pH of the solution to be degraded, and the pH of the precursor solution (catalyst's solution during preparation of catalyst); effect of dye concentration and effects of amount of catalyst.

a. Effect of pH

In heterogeneous photocatalytic system, pH is one of the most important operating parameters that affect the charge on the catalyst particles, size of catalyst aggregates and the positions of conduction and valence bands. Photocatalytic degradation efficiency of dyes is significantly affected by pH value of the solution. The surface charge of catalyst particles are changed at a different solution of pH and shifts to the potentials of catalytic reactions. As a result, the adsorption of dye on the surface TiO_2 photocatalyst can be altered thereby causing a change in the reaction rate. At higher pH, there is excess of OH^- anions, which facilitate photogeneration of hydroxyl radicals. Change in pH shifts the redox potentials of valence and conduction bands, which may affect interfacial charge transfer [41].

b. Effect of Concentration

The quantity of the dye adsorbed on the surface of TiO_2 photocatalyst is of foremost importance since only this amount contributes to photocatalytic process and not the one in the bulk of the solution. The extent of dye adsorption depends on the dye initial concentration. Generally speaking the percentage degradation decreases with increasing amount of dye concentration, while keeping a fixed amount of photocatalyst [42].

c. Effect of Photocatalyst Dosage

Several studies have indicated that the photocatalytic rate initially increases with catalyst loading and then decreases at high values because of light scattering and screening effects. The tendency toward agglomeration (particle-particle interaction) also increases at high solids concentration; resulting in a reduction in surface area available for light absorption and hence a drop in photocatalytic degradation rate. Although the number of active sites on the surface of TiO_2 will increase with catalyst loading, a point appears to be reached where light penetration is compromised because of excessive particle concentration [43].

d. Effects of Reaction Temperature

An increase in reaction temperature generally results in increased photocatalytic activity however reaction temperature >80°C promotes the recombination of charge carriers and disfavor the adsorption of organic compounds on the Titania surface. A reaction temperature below 80°C favors the adsorption whereas further reduction of reaction temperature to 0°C results in an increase in the apparent activation energy. Therefore temperature range between 20-80°C has been regard as the desired temperature for effective photo mineralization of organic content [44].

2.3.4 Surface Modification of TiO_2 Nanoparticles

The band edges of this semiconductor nanoparticle lie in the UV region which makes them inactive under visible light irradiation. Researchers have been interested in the modification of electronic and optical properties of this metal oxide nanoparticles for their efficient use in water and air purification under visible light irradiation. Visible light activity has been induced in TiO_2 by surface modification via organic materials/semiconductor coupling and band gap modification by doping with metals and nonmetals, co-doping with nonmetals, creation of oxygen vacancies and oxygen sub-stoichiometry [45].

Fujishima and Honda first demonstrated that TiO_2 was a promising photo-anode for UV light- driven photocatalytic water splitting, which has been widely studied in many photocatalytic reactions due to its chemical stability, low cost, environmentally friendly nature, and tunable electronic energy band gap. Figure 6 shows a band gap illustration of TiO_2 [46].

The valence band of TiO_2 is more positive than E^0ox of O_2/H_2O (1.23 V vs. NHE, pH = 0), while the conduction band is more negative than E^0red of H^+/H_2 (0 eV vs. NHE, pH = 0). However, TiO_2 materials suffer from two major drawbacks. One is the fast charge carrier recombination, which results in the release of unproductive energy. Another one is the inability to harvest visible light, since TiO_2 can only be excited by UV light due to its wide band gap of 3.0–3.2 eV, which only covers 5% of the solar spectrum. To enable visible light harvesting and prevent the recombination of photogenerated electron-hole pairs, proper modification should be performed. In this section, suitable modification methods will be introduced, including doping, making heterojunctions with other semiconductors or metals, and structural changes [47].

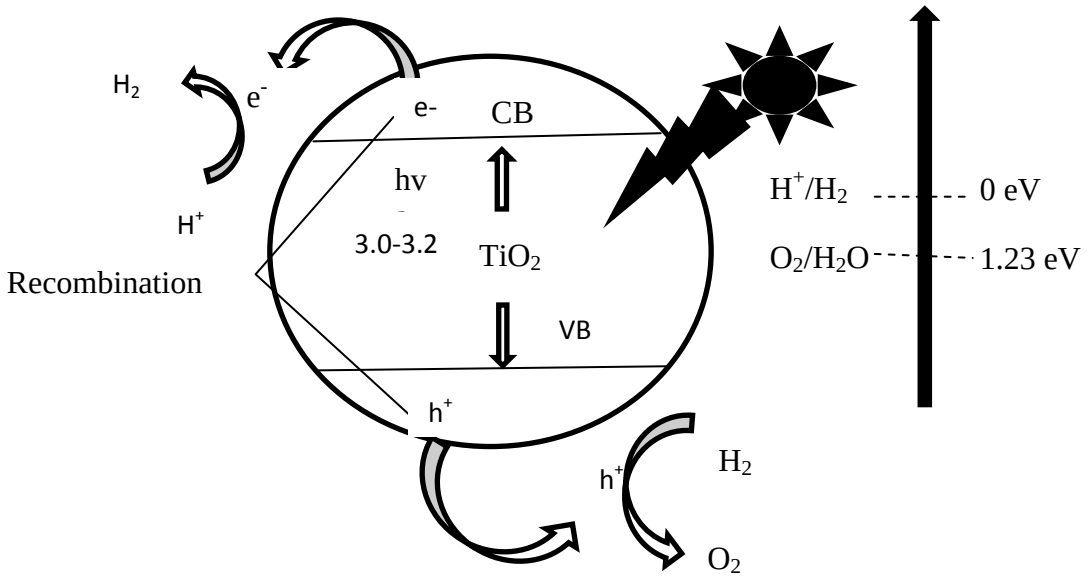

Figure 7 . Schematic band gap diagram of TiO_2 [47].

a. Metallic Doping

The most detrimental aspect of the photoactivity of TiO_2 is its relatively high electron-hole recombination rate. Previous studies demonstrated that the appropriate amount of metals doped on TiO_2 could inhibit the recombination of photo-induced electron-hole pairs. The change in electronic properties of TiO_2 by substitution of metal ion for Ti^{4+} sufficiently reduced the energy band gap to absorb visible light. Many studies were reported for the characteristic behavior of visible active metal doped semiconductor photocatalyst where the dopants include noble metals, rare earth metals, and transition metals, and so forth. Silver and gold nanoparticles possess additional ability to absorb visible light, due to localized surface Plasmon resonance (an optical phenomena generated by a light wave trapped within conductive nanoparticles smaller than the wavelength of light),which again

contributes to the visible light activity, when the noble metals are doped over TiO_2. For example Vanadium dopant is accounted as one of the best metal dopants to extend the optical absorption of TiO_2 towards the visible light region. The enhanced absorption to visible light region and improved quantum efficiency, owing to the improvement in e^-- h^+ pair separation makes TiO_2 an efficient photocatalyst in the presence of vanadium [48].

b. Non-metallic Doping

Considerable efforts have been made to extend the photoactivity of TiO_2 based systems into the visible light region for the efficient utilization of solar energy. Nonmetal doping is an alternative for improving the visible light response of TiO_2, and extensive research work has been done on synthesis of N-doped, S-doped, F-doped, and C doped TiO_2. The doping with nonmetal could narrow down the band gap by modifying the electronic structure around the conduction band edge of TiO_2, by incorporating anion into the crystal lattice of TiO_2. This might drive better photocatalytic performance under visible light. Recently, many researchers paid much attention to nitrogen-doped TiO_2, which can be produced using different techniques, such as hydrolytic process mechanochemical technique. Nitrogen can be easily introduced in the TiO_2 structure, due to its comparable atomic size with oxygen, small ionization energy and high stability [49]. Figure 8 here shows the electron transfer mechanism of N - doped anatase - rutile heterojunction.

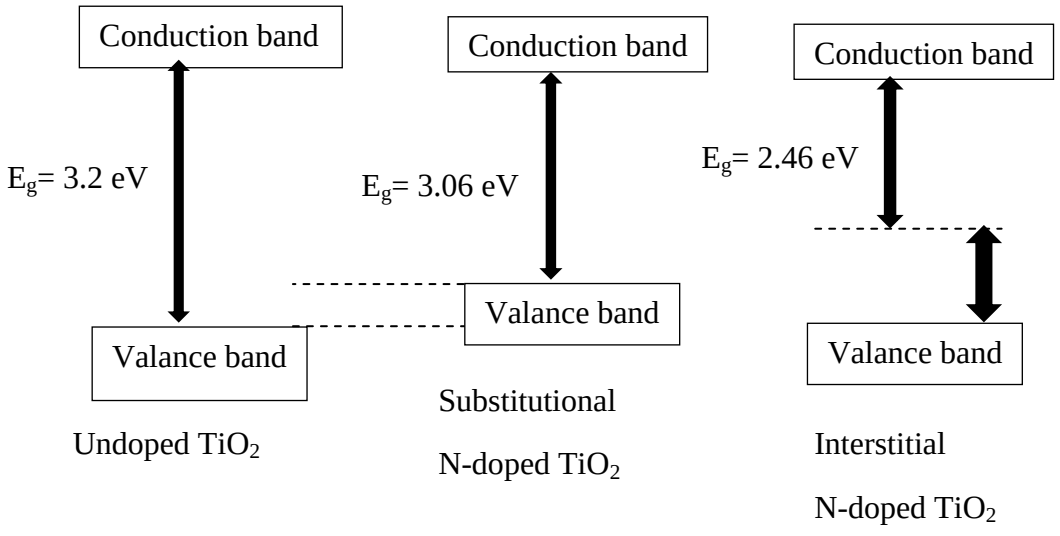

Figure 8. Electron transfer mechanism in N-doped anatase - rutile heterojunction [50].

c. Doping TiO_2 with Electron Donating Conducting Organic Polymers

In recent times, some studies have been done on the combination of conductive polymers and TiO_2 to get better performance of UV light and visible light activities. Moreover, many conjugated polymers also are efficient electron donors and good holes transporters upon visible light excitation. Therefore, conjugated polymers with large band gap inorganic semiconductors obtain awareness for optical, electronic, photocatalytic and photoelectric conversion applications. In spite of many reward of TiO_2, its photocatalytic water-splitting efficiency under solar energy is still somewhat low, mainly owing to the following reason [51].

2.4 Graphene Nanoparticles

Graphene has sp^2 hybridized planar honeycomb lattice structure with zero energy band gap and having remarkable properties such as high conductivity, large surface area, high mechanical and thermal stability. These properties offer Graphene valuable materials in various applied research such as in fuel cell catalysis, super capacitor, photocatalysis, heterogeneous catalysis, water purification, drug delivery and biosensing [52].

In particular high charge carrier mobility (up to 105 $cm^2\ V^{-1}\ s^{-1}$, high intrinsic strength (130 GPa), high thermal conductivity at room temperature (103 $Wm^{-1}\ K^{-1}$ and large surface area (>2000 $m^2\ g^{-1}$ compared to graphite (10 $m^2\ g^{-1}$ or carbon nanotube (1300 $m^2\ g^{-1}$ have been utilized to make graphene based nanocomposite for optical and electronic application. In addition it is reported that the efficacy of graphene based materials is generally higher as compared to other forms of carbon such as carbon nanotube and fullerene [53].

Graphene is highly hydrophobic in nature, does not dissolve in hydrophilic solvent and forms large aggregates via – interaction/van der Waals interaction. In order to overcome this issue Graphene oxide (GO) is commonly used as alternative. The chemical exfoliation of graphite powder by strong oxidizing reagent produces highly colloidally stable exfoliated sheets of hydrophilic GO. GO contains carbons with sp^2 (C=C, C=O etc.) and sp^3 (C–C, C–OH, C–O–C etc.) hybridization and with oxygen functionality such as hydroxyl, epoxy, carbonyl and carboxyl groups. However, unique properties of graphene are compromised in GO, that limits its use particularly, in electronic or energy based applications. In contrast, colloidal GO offers opportunities for functionalization with

molecules/polymers/metal nanoparticles and extends the application potential. GO can be transformed into reduced Graphene oxide (RGO) by providing thermal, chemical, photochemical and electrochemical reducing atmosphere. This processes increases the number of sp^2 hybridized carbon atoms and greatly recovered the lost properties of graphene. The RGO has enhanced self-aggregation processes and lower solubility but with enhanced conductivity, light absorption property, mechanical and thermal stability. Quality of RGO depends on the processes and nature of reducing agents. Similar to GO, RGO is also widely used in preparation and processing of graphene based composites [54].

Nanoparticles are widely used in optical, biomedical and electronic application. Commonly used nanoparticles include metal/metal oxide nanoparticles (e.g., Pt, Pd, Co_3O_4, Au, Ag), semiconductor nanoparticles (e.g., TiO_2, CdSe, ZnS, ZnO) and magnetic nanoparticles (e.g., Fe_2O_3, Fe_3O_4. The semiconductor nanoparticles have definite energy band gap suitable for absorbing/emitting light in the UV-visible range and acts as photocatalyst [55].

A Graphene-nanoparticle composite offer the property of both component and remove some of the limitations of individual components and in some cases enhances the performance of individual component. In continuation on focusing of nanoparticle based composites with other carbon based materials such as carbon nanotube and fullerene, the graphene based similar composites offers better performances in most of the applications. The nanoparticles are linked with graphene through hydrophobic, electrostatic interaction or covalent bonds and synergistic effect prevents the stacking between graphitic sheets as well as aggregation between nanoparticles. Recently several reviews appears on graphene based composites with nanoparticle and polymer, focusing mostly on synthesis and property and limited attention is paid on application potential. In this review, we will focus mostly on the application potential of graphene-nanoparticle composites towards the biomedical, electronic, catalytic, energy and environment based applications [56].

Chemical structure of graphene, GO, RGO and G-N composites are shown in Figure 9. High quality graphene is generally synthesized by micromechanical exfoliation on silicon substrate or chemical vapour deposition on transition metal surfaces but these methods have low production efficiency. In addition insufficient functional groups generated on graphene surfaces limits preparation of graphene based nanocomposites. Thus colloidal GO, prepared by Hummer's method or modified Hummer's method, are commonly used

for large scale synthesis of graphene based composites. Figure 10 summarized different synthetic [57].

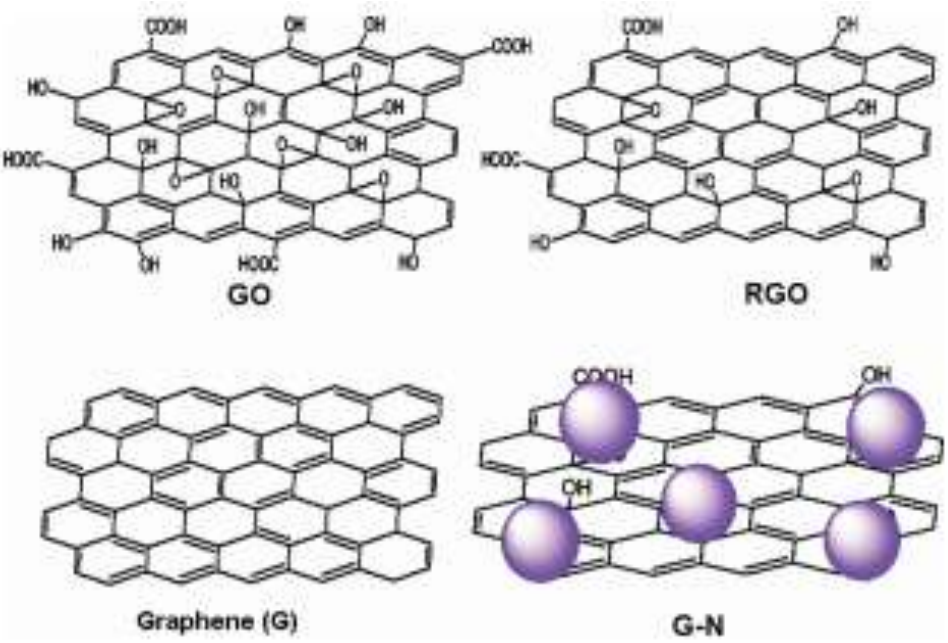

Figure 9. Chemical structure of graphene oxide (GO), reduced graphene oxide (RGO), graphene and graphene-nanoparticle (G-N) composites [57].

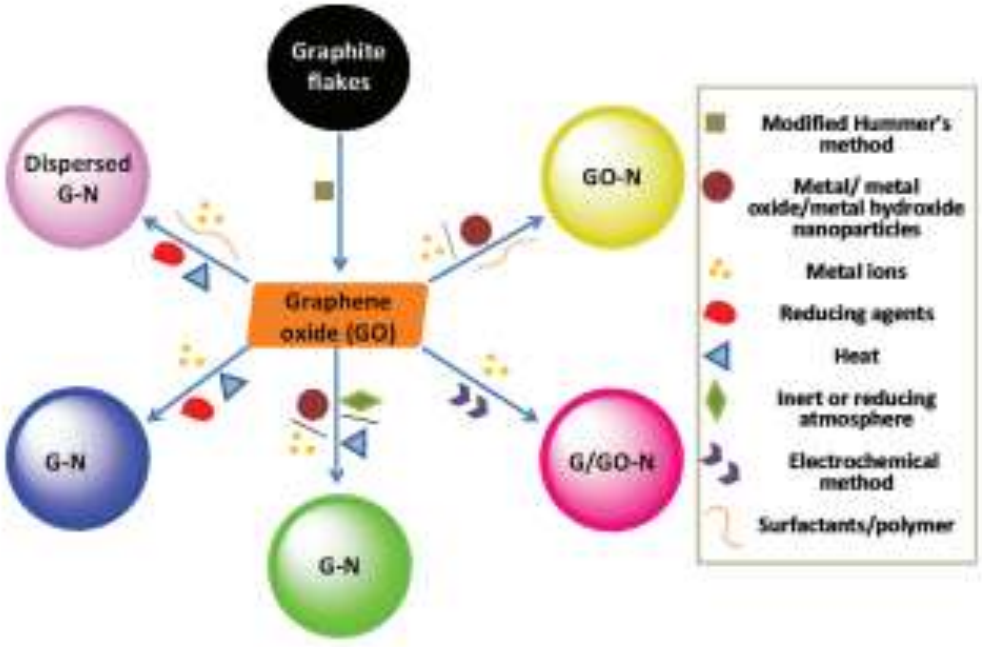

Figure 10. Schematic illustration of synthetic strategies for graphene/GO based composites with different nanoparticles [58].

2.5 Nanocomposites

Nanocomposites are those composites in which one phase has nanoscale morphology like nanoparticles, nanotubes, or lamellar nanostructure. They have multiphase, so are multiphasic materials, at least of the phases should have dimensions in the range of 10–100 nm. To overcome the limitation of different engineering materials now-a-days, nanocomposites are emerged to provide beneficial alternatives. Nanocomposites can be classified on the basis of their dispersed matrix and dispersed phase materials. With the help of this rapidly expanding field, now-a-days, it has been possible to generate many exciting new materials with novel properties via innovative synthetic approaches. The properties of the so-called found not only depended on the properties of their originals, but also crucially on their interfacial and morphological characteristics. Of course, we cannot ignore the fact that sometimes it also happened that the newly generated property in the material is unknown to the parent constituent materials. Hence, the idea behind nanocomposites is to use building blocks with dimensions in nanometer range to design and create new materials with unprecedented flexibility and improvement in their physical properties [59].

Nanocomposites are the solid combination of a bulk matrix and nanodimensional phase(s) which differ in properties due to dissimilarities in structure and chemistry. Properties that have indicated substantial improvements: Mechanical properties (strength, bulk modules, withstands limit, etc.), thermal stability, hinders flame and reduce smoke generations, permeability of gases, water, and solvents are reduced, more surface appearance, improved electrical conductivity, increased chemical resistance and enhance optical clarity as compared to conventionally filled polymers [60].

Among several nanocomposites, polymer-based nanomaterials are the most leading materials of current research and development. Characteristics like film forming ability, activated functionalities, and dimensional variability provide lots of benefit to polymer-based nanocomposites [61].

Nanocomposites can be formed by blending inorganic nanoclusters, fullerenes, clays, metals, oxides, or semiconductors with numerous organic polymers or organic and organometallic compounds, biological molecules, enzymes, and sol-gel derived polymers.

Nanocomposite materials that are obtained by the combination of two or more separate building constituents in one material offers unique properties that plausibly arises from their small size, large surface area, and off course from the interfacial interaction between the phases. Their extra ordinary potential have been smoothly utilized to enhance the biological potential of many drugs, biomaterials, catalysts, and also in some high-value added materials [62].

Nanocomposite materials can be classified in the following way based on the presence or absence of polymeric material in the composite. The nanocomposites in which the compositions do not contain any polymers or polymer-derived materials are called non-polymer-based nanocomposites (Figure 11). Non-polymer-based nanocomposites are also known as inorganic nanocomposites. They can be further classified into metal-based nanocomposites, ceramic-based nanocomposites, and ceramic-ceramic-based nanocomposites [63].

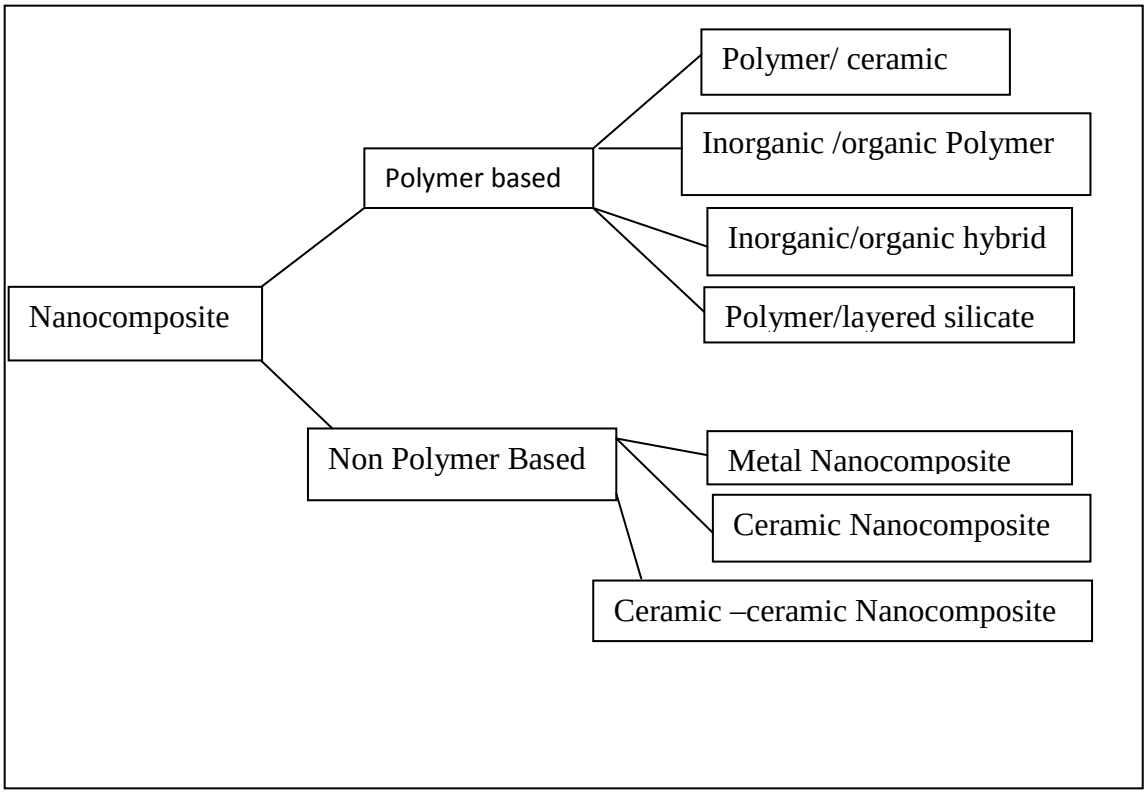

Figure 11 Classification of nanocomposite as polymer and non-polymer based [63].

2.5.1 Titanium Dioxide/Reduced Graphene Oxide (TiO_2/rGO)

Among the different nanomaterials graphene has emerged as one of the most prospective nanomaterials due to the unique combination of its exotic properties. Based on the binder material graphene nanocomposite can be categorized as graphene metal/metal oxide nanocomposite, graphene ceramic nanocomposite, graphene semiconductor nanocomposite and graphene polymer nanocomposite. Among various nanocomposites, graphene-metal/metal oxide composites have attracted considerable attention because of their potential applications in energy and health related areas [64]. Figure 12 depicts surface modifications of Graphene that increases energy band gap.

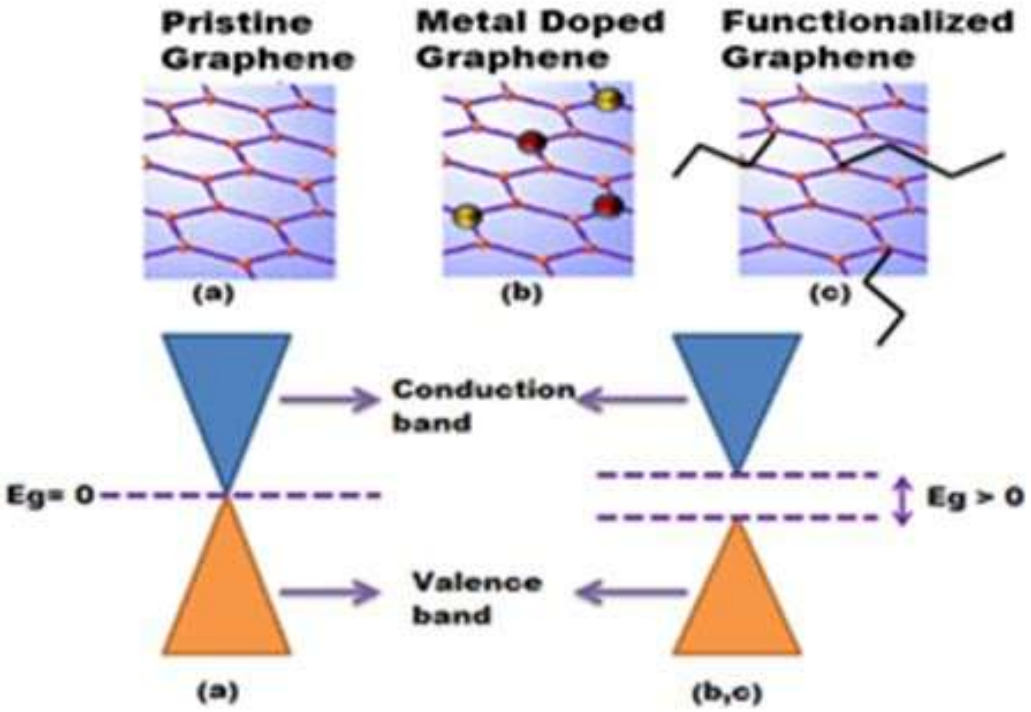

Figure 12. Surface modifications of Graphene that increases energy band gap [65].

There are three basic methods (physical, chemical and biological) to synthesize TiO_2r/GO nanocomposites such as sol-gel, solution mixing, hydrothermal/ solvothermal, self-assembly, microwave irradiation and others. Among this sol-gel method is the best route due to its simplicity and inexpensive nature [66]. Figure 13 shows schematic illustration of binding mechanisms of the nanoparticles onto rGO.

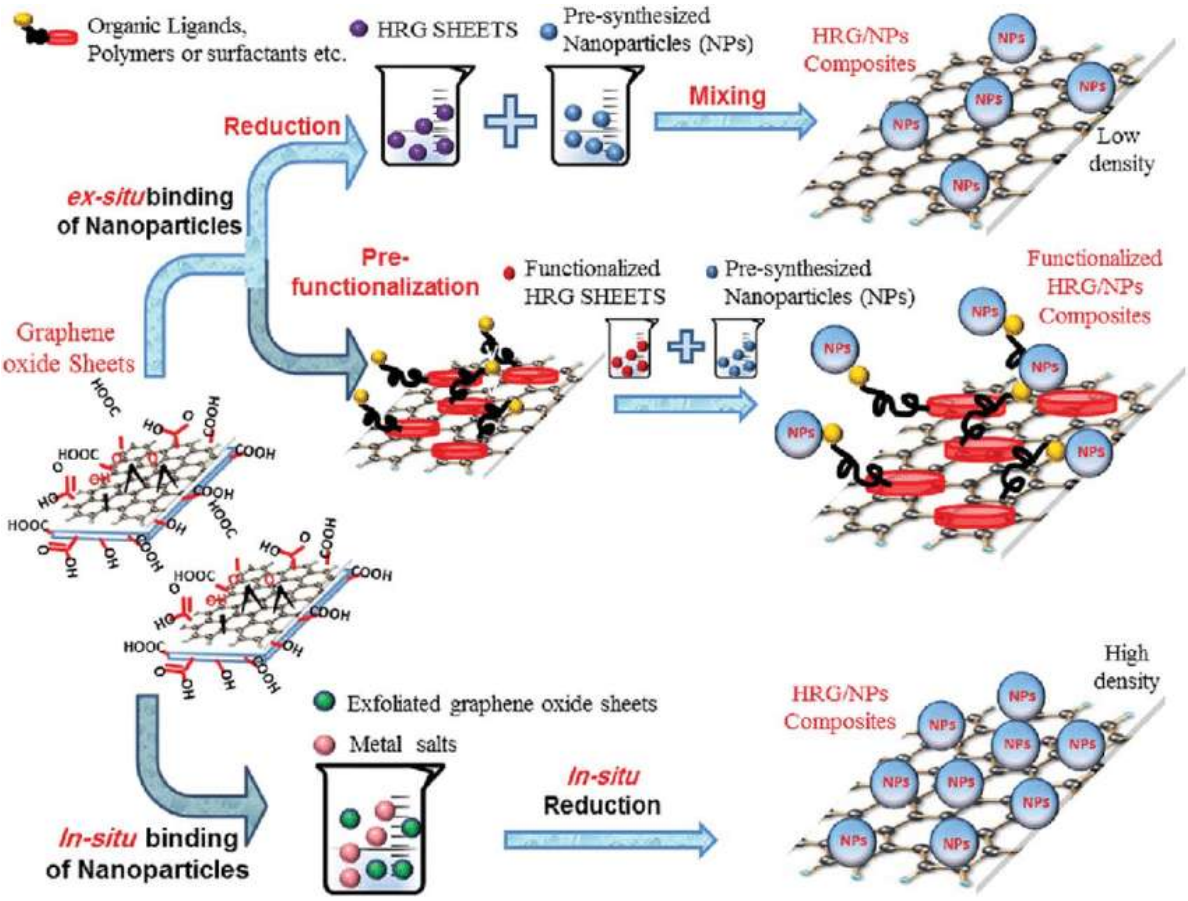

Figure 13. Schematic illustration of binding mechanisms of the nanoparticles onto rGO [67].

From the above methods; sol–gel route provides simple, inexpensive preparation of a homogeneous composite material with excellent compositional control and thus used in many applications. Zhang et al. [57] used tetrabutyltitanate and GO as the starting materials for the sol gel synthesis of rGO/TiO_2 nanocomposites and found that the photocatalytic activity of the composite was affected by both graphene content and the calcinations atmosphere [68]. Li et al. [67] used sol gel method to ultra-disperse TiO_2 nanoparticles on graphene with extreme control so that the grown material can achieve twice the specific capacity as that of mechanically mixed composites.

2.6 Photocatalysis

Photocatalysis is an environmentally benign process involving the conversion of light energy into chemical energy under ambient conditions. The outstanding performance of solar driven photocatalytic processes in solving environmental problems has gained much attention in recent years. Effluents from the textile and paint industries are the main

sources of environmental organic contaminants. Thus, it is essential that the latter is degraded and converted into harmless mineral compounds [69].

The photocatalyst can be harnessed for environmental remediation, which includes abstraction of pesticides, fungicides and fertilizers from wastewater and the eradication of organic pollutants from the air Activation of a semiconductor photocatalyst is achieved by the absorption of a photon, which results in the transfer of an electron from the valence band to the conduction band by creation of a hole ($h^{+)}$ in the valence band. These photo-generated charge carriers cause redox reactions on the surface of the photocatalyst, i.e., any contaminant that is adsorbed onto the photocatalyst surface will undergo reduction or oxidation by the electron-hole pair respectively [70].

Generally, the metal oxide photocatalyst surface acts as an active center in photocatalysis, either by the generation of OH· radicals (by oxidation of OH^- anions) or by the generation of O_2^- radicals (by the reduction of O_2·). Subsequently, these photo-generated radicals and anions react with the adsorbed organic contaminants, degrading or mineralizing them into less harmful by-products. The photocatalytic reaction can be employed to bring about the transformation of highly toxic chemicals into less noxious or non-toxic products such as CO_2 and H_2O. Consequently, metal oxides can be employed as prime candidates for the effective photocatalytic degradation of environmental contaminants [71].

The proposed mechanism of dye degradation is shown in Figure 14 by absorbed light, valence electrons of TiO_2 excited to the conduction band. RGO can act as electron trap and the photogenerated electrons can be transferred to the rGO. The trapped electrons on rGO can react with the dissolved oxygen to form reactive oxygen species. In this way, electron−hole recombination rate decreases. The photogenerated electrons on the TiO_2 surface could also be trapped directly by the dissolved oxygen to form reactive oxygen species, which react with water to give hydroxyl radicals. The dye is then degraded by the hydroxyl groups. On the other hand, holes on the valence band of TiO_2 react with absorbed water or hydroxyl groups to form surface hydroxyl radicals which then degrade dye. The holes can oxidize the dye molecules directly. The main reactions are shown below [72].

TiO_2 /RGO → TiO_2 (h^+) - RGO (e^-)……9

RGO (e-) + O_2 → RGO + $^-O_2$……...10

TiO_2 (h+) + H_2O ($^-$OH) → TiO_2 + ·OH.....11

·OH + MB → CO_2 + H_2O..……12

In this study, we have focused on the green synthesis of TiO_2/rGO nanocomposite and their effective application in the photocatalytic degradation of a commercially used organic dye, methylene blue. The influence of various parameters such as: solution pH values of organic dyes, initial concentration, aging time and catalysis doze on photocatalytic efficiency were also studied [73].

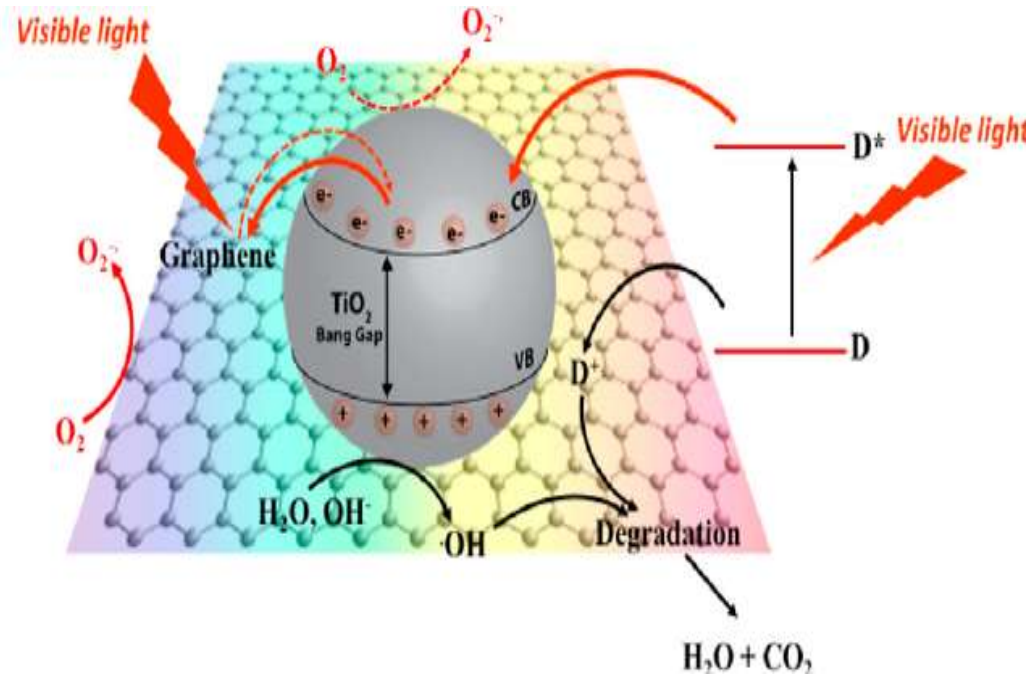

Figure 14. Mechanisms of UV and visible light activation of TiO_2 with G in the presence of dye (D) [73].

3. MATERIALS AND METHODS

3.1 Chemicals and Reagents

All chemicals including Titanium tetrabutoxide ($Ti(OC_4H_9)_4$ 97% Sigma-Aldrich, India), Sulfuric acid (H_2SO_4 98%, Sigma-Aldrich, India), phosphoric acid (H_3PO_4 ,65%, Sigma-Aldrich, India), hydrochloric acid (HCl 36-38%, Sigma-Aldrich, India), hydrogen peroxide (H_2O_2 30% Sigma-Aldrich, India), potassium permanganate ($KMnO_4$ LR, Alpha), Barium chloride ($BaCl_2$ LR Alpha), methylene blue ($C_{16}H_{18}ClN_3S$ LR, LOBA Chemia), ethanol (C_2H_5OH 97%, Silva, Ethiopia) and graphite powder (diameter 6 mm, 99.995% trace metals basis, Sigma-Aldrich, India) were purchased and used as received.

3.2 Collections of Orange and Banana Waste Fruit Peels

Fresh *Citrus aurantium* (Orange) and musa acuminata (banana) fruits were collected from Adama City, Oromia Region, Ethiopia. The samples were washed with tap water three times followed by distilled water to remove dust particles. The peel parts were taken by using knives from each fruit, and labeled and completely dried in open air under shade for about two weeks. Then, the samples were crushed and grinded using electrical supper blender to produce a fine powder.

3.3 Aqueous Extraction of Citrus Aurantium and Musa Acuminata

15 g of the *citrus aurantium* powder was taken in to 500 ml of conical flask and 250 ml of distilled water was added. Then, covered with aluminum foil and heated at a constant temperature of about 70°C for 30 minutes and stirred using a magnetic stirrer at 1000 rpm. The mixture was cooled and filtered using Watchman filter paper (125 mm diameter) to remove residue from the mother liquor. Finally, the pale yellow filtrate was stored at 4°C for further use. The same procedures were repeated using *musa acuminata* and brown filtrate was obtained [74].

3.4 Green Synthesis of TiO_2 Nanoparticles using CA and MA Extracts

TiO_2 nanoparticles were synthesized by sol-gel method using Titanium (IV) Tetra-butoxide ($Ti(OC_4H_9)_4$) as a precursor. In typical procedure, a mixture of ($Ti(OC_4H_9)_4$) with ethanol was stirred for 30 minutes to obtain 0.1 M of 100ml solution. To this precursor sol, distilled water extract of *Citrus aurantium* was added drop wise. The ratios V/V of

precursor to plant extracts were: 1:1 (TiO_2-1c), 1:2 (TiO_2-0.5c) and 2:1 (TiO_2-2c). The solutions were stirred using magnetic stirrer for 5 hours at room temperature. The solutions were settled overnight, and the residue part were centrifuge at 1000 pm for 10 minutes followed by washing using water and ethanol three times sequentially, to remove impurities. The product was dried at 100ºC for 12 hours in the oven and calcinated at 500^{o}C for 4hrs in muffle furnace. The same procedure was followed to synthesis TiO_2-1m, TiO_2-0.5m and TiO_2-2m NPs using *musa acuminate* extract. The white TiO_2 nanoparticles were preserved for the next characterization and synthesis of TiO_2/rGO nanocomposite [75].

3.5 Synthesis of Graphene Oxide (GO)

Synthesis of GO was carried out by Tour Method [76]. The synthesis procedure involves oxidation of graphite using strong oxidizing agent using $KMnO_4$ in the presence of H_3PO_4, which acts as prevention of further oxidation [77]. 0.5 g of graphite powder was exfoliated using 90 ml H_2SO_4 in presence of H_3PO_4 at 0^{o}C under ice bath, followed by gradual addition of 4.5 gm $KMnO_4$ in small portion. After the addition of $KMnO_4$, the solution was stirred for 8 hours while heating to 50 ^{o}C using a temperature controlled water bath. As the reaction time was extended, the mixture turned out to paste. The reaction was terminated by addition of 250 mL of distilled water followed by 10 mL H_2O_2 (30%) solution. The purpose of H_2O_2 was to reduce residual $KMnO_4$ to soluble manganese sulfate ($MnSO_4$) in an acidic medium as described in the following reaction:

$$2KMnO_4 + 5H_2O_2 + 3H_2SO_4 \longrightarrow 2MnSO_4 + K_2SO_4 + 8H_2O\ (steam) + 5O_2$$

When 30 wt. % H_2O_2 was added, bubbling occurred and a bright yellow color was observed, indicating a high level of oxidation. The solution was then filtered using the filter paper to remove the metal sulfate and a graphite oxide filter cake was produced. The cake was washed with 5% HCl aqueous solution until the sulfate ions are removed completely. The removal of the metal sulfate ions was confirmed using $BaCl_2$ solution. The washing process was carried out three times by centrifugation at 1000 rpm for 30 minutes and the supernatant was decanted away. The collected material was checked using a universal indicator and found to be pH 7. The collected material (graphite oxide) was added to 100 ml of distilled water and stirred followed by heating at 60°C for 8 hours in a water bath. The brown color of GO solution was dried at 60 ^{o}C for 6 hours in oven drier [78].

3.6 Synthesis of TiO_2/rGO Nanocomposite by Co-precipitation Method

TiO_2/rGO nanocomposite was prepared using synthesized GO, TiO_2 and, *citrus aurantium* (CA) and *musa acuminate* (MA) extracts as reducing agent by precipitation technique [75]. In the typical synthesis, GO suspension was prepared by dispersing dried 30, 60 and 90 mg powders in 100 ml of distilled water via sonication. Subsequently, 60 mg of TiO_2 and 50 ml of CA extracts were added to the GO slurry and stirred for 8 h at room temperature. Then, the solution turned to grey from brown colors indicating the reduction of GO to reduced graphene oxide. The grey residue of rGO/TiO_2-0.5c, rGO/TiO_2-1c and rGO/TiO_2-1.5c were then centrifuged for 30 minutes and washed three times by water and ethanol sequentially. The obtained material was kept in vacuumed oven at 100^0C for 24 hours. The same procedure were repeated for *musa acuminate* extract and assigned as TiO_2/rGO-0.5m, TiO_2/rGO-1m and TiO_2/rGO-1.5m nanocomposites.

3.7 Characterizations of Synthesized TiO_2 NPs and TiO_2/rGO nanocomposite

3.7.1 Thermal Gravimetric -Differential Thermal Analysis (TGA-DTA)

TGA (DTG-60H, SHIMADZU Corporation, Japan) is the analysis of the change in the mass of a sample on heating.TG measures mass changes in a material as a function of temperature under a controlled atmosphere and used to determine the changes in weight of the sample with increasing temperature. Differential thermal analysis (DTA) is the most widely used thermal method of analysis in which the temperature of a sample is compared with that of an inert reference material during a programmed change of temperature, so provide valuable information about the energy gain or loss during the process. Therefore, the TGA-DTA analysis of the samples was carried out to determine calcination temperature.

3.7.2 X-Ray Diffraction (XRD) Analysis

To characterize crystal structure and phase of TiO_2 NPs and TiO_2/rGO nanocomposite, small amount of the powders were taken and grounded to fine particle and analyzed by XRD (XRD-7000, SHIMADZU Corporation, Japan) equipped with a Cu target for generating a Cu Kα radiation with $\lambda = 0.15406$ nm. The 2θ record range from 10^0– 80^0 while the accelerating voltage and applied current is held at 40 kV and 50 mA, respectively. The particle size (D) of the powders was calculated by using Scherer's Formula;

$$D = \frac{k\lambda}{\beta cos\theta} \quad \text{.....13}$$

Where, D is crystallite size in nanometer, k is shape factor constant, which is 0.89, β is the full width at half maximum (FWHM) in radian, λ is the wave length of the X-ray and θ is the Bragg angle [45] .

3.7.3 Fourier Transformer Infrared (FT-IR) Spectroscopy Analysis

FT-IR measurements were performed to identify the possible significant functional groups that were responsible for reducing and capping of rGO, TiO_2 and TiO_2/rGO nanocomposite. Furthermore, FT-IR spectra were used to identify the characteristics peak of Ti-O and Ti-O-C bindings. FT-IR spectra of the biosynthesized TiO_2/rGO nanocomposite were recorded at room temperature using a FT-IR spectrophotometer (FT/IR-6600typeA, Jasco Company, Japan) in order to analyze and detect surface functional groups at the scanning range of 4000 – 400 cm^{-1}. For FT-IR measurements, a small amount of powdered orange peel, banana peel, GO, rGO, TiO_2 and TiO_2/rGO nanomaterials were pelleted with standard KBr powder.

3.7.4 Scanning Electron Microscope (SEM) Analysis

Morphologies and elemental mapping analysis of the samples was investigated by using SEM (JCM-6000plus BENCH TOP SEM, SHIMADZU Corporation, Japan) instrument operating at constant beam energy.

3.8 Optical Properties

By using UV-Vis spectroscopy Diffuse reflectance mode (OPTIMA UV-Vis spectrometer SP-3000 Plus, SHIMADZU Corporation, Japan), the energy band gaps (E_g) of the nano-powders (TiO_2 and rGO/TiO_2) were estimated in the wave length range of 200–800 nm. First, the reflectance of the powders at Kubelka-Munk (K-M) units was measured. The application of the K- M method is based on the equations 14 and 15 below:

$$[F(R)hv]^n = A(hv - E_g) \quad \text{.....14}$$

$$(R) = \frac{1-R^2}{2} \quad \text{.....15}$$

Where R is the reflectance, Eg is the energy band gap, α is the absorption coefficient, h is Planck's constant, ν is frequency, A is a constant, and n = 1/2 for direct applying the K-M

method, the band gap energy can be obtained by extrapolating the linear region of the spectra (F(R) hv) 1/2 vs. hv [79] . This method is usually applied when the samples measured exhibit high absorbance or light scattering.

3.9 Photocatalytic Degradation Studies of Methylene Blue

The photocatalytic activities of TiO_2 and TiO_2-rGO were tested in 125 ml of Pyrex flask type reactor under 150W halogen lamp irradiation. 20mg of catalysts were introduced into 120 ml aqueous solution of methylene blue (20mg/l, pH 6.8). In each experiment, in order to reach the adsorption-desorption equilibrium, the solutions was kept in the dark for 10 minutes before irradiation. The light source was positioned on top of the solutions and all the samples were irradiated under continuous stirring. The decomposed dye solutions were centrifuged at 1000 rpm for 30 min and for the measurement of Double Beam UV-visible Spectrophotometer (SM-1600 spectrometer MAALAB, India). The photo-degradation rate of methylene blue (MB) was calculated by the following equation 16:

$$\text{Degradation (\%)} = \left(\frac{A_o - A_t}{A_o}\right) * 100 \quad \text{.....16}$$

Here A_o is the initial concentration of dye and A_t is the concentration at desired time. All concentration values were obtained by the maximum absorption 664 nm for methylene blue in the absorption spectrum.

The effects of catalyst dosage (10, 30 and 50mg), pH (1, 7 and 13); concentration of methylene blue (10, 20 and 30 mg/l) and visible irradiation time (10-60min) were investigated by using TiO_2/rGO-1.5c catalyst for degradation of methylene blue. According to first order kinetics reaction, rate constant k (min^{-1}) was determined by using the following equation 9 [80]:

$$\ln\left(\frac{C_t}{C_o}\right) = -kt \quad \text{.....17}$$

Where C_o and C_t are concentration at the beginning and at a certain time, t is the irradiation time. The temporal changes of MB concentration (C_t/C_o) were proportional to maximum absorbance (A_t/Ao, λ = 664 nm).

4. RESULTS AND DISCUSSION

The dark brown GO well dispersed into water to form a homogeneous and stable solution owing to the presence of a lot of oxygen-containing groups such as -OH, C=O, C-O-C, and -COOH. Solution is cake yellow, in good agreement with the reported results [76]. The white colors of prepared TiO_2 NPs powder were taken as 60 mg from both extract synthesis. TiO_2 nanoparticles, a well-known photocatalyst, usually have a good dispersion in the aqueous solution. After addition of 50 ml citrus aurantium and musa acuminata extracts were grey precipitate of TiO_2/rGO nanocomposite were obtained for both extracts sequentially. Further observation indicates that after the precipitation of the TiO_2/rGO composite, the resident solution is very clear and colorless suggesting that the rGO nanosheets in the solution are completely coupled on the surface of TiO_2 nanoparticles to form a TiO_2-rGO composite.

4.1TGA/DTA Analysis

The thermal decomposition, phase transition and phase stability of synthesized TiO_2 nanoparticles were studied by TGA/DTA analysis. They are widely used to evaluate the thermal stability of materials. The TGA/DTA graphs of TiO_2 nanoparticles synthesized by CA and MA extract were shown in Figure 15. TiO_2 nanoparticles weight losses were occurred in three stages for both extracts synthesized. The first stage weight loss was observed between 40-125 ^oC which are attributed to the removal of water or moisture content. The second stage weight loss was observed between 125-503 ^oC which are corresponding to losses of organic residues and organic molecules/compounds as a result of combustion. The third weight losses observed in the range 503–800 ^0Ccould be probably due to the phase transformation of amorphous to crystalline anatase phase. Furthermore, the DTA curve distinctly shows two exothermic peaks and one endothermic peak. The first and second peaks at 106.63 $^\circ C$ and 303.77 $^\circ C$ are due to the removal of water and residual organic compounds, respectively while the second sharp peak at 521 ^oC is due to the crystallization of TiO_2. As it can also be observed from TGA/DTA analysis result, the synthesized TiO_2 NPs are thermally stable for temperature ranges above 550 ^oC.

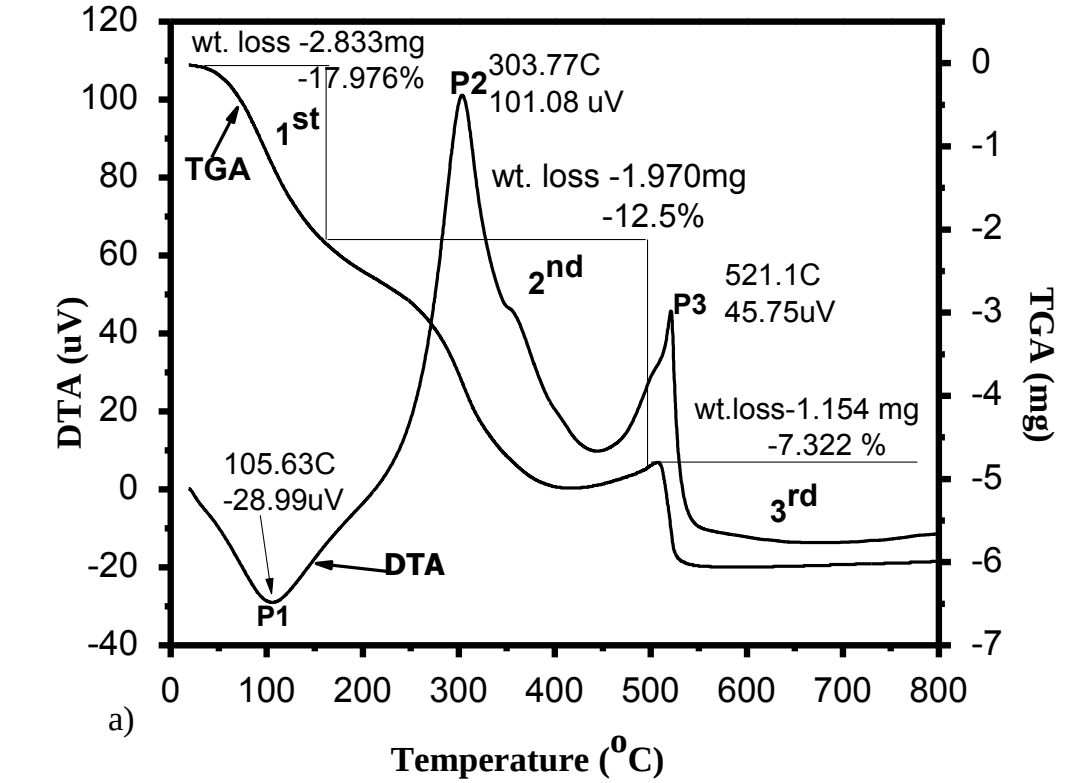

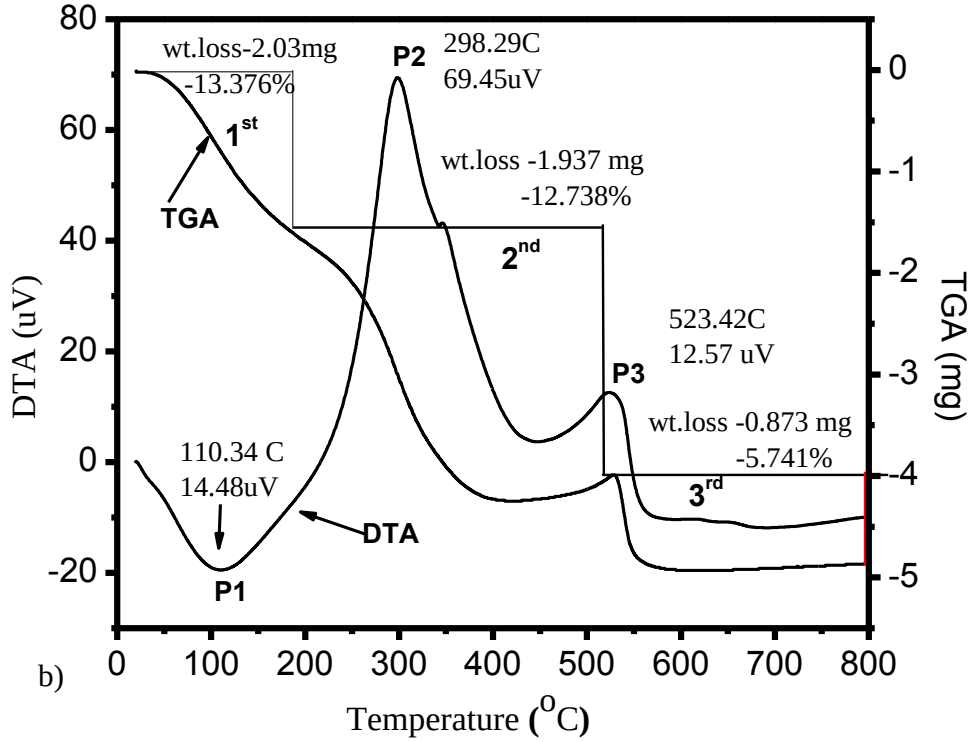

Figure 15. TGA-DTA of TiO_2 nanoparticles synthesized using a) *citrus aurantium* and b*) musa acuminata* extracts.

4.2 XRD Analysis

Figure 16 shows XRD patterns of GO, rGO, TiO_2 NPs, and rGO/TiO_2 nanocomposites. As we observed from Figure 16 (a and b), TiO_2-1c, TiO_2-2c, TiO_2-1m and TiO_2-2m shows diffraction peaks at 2θ=25.3°, 38.4°, 48.55°, 55.55°, 62.66°, 69.77° and 75.29° indexed to the crystalline planes (1 0 1), (0 0 4), (2 0 0), (1 0 5), (2 0 4), (1 1 6) and (2 1 5) respectively which correspond to the standard pattern of the an anatase crystalline phase of TiO_2 JCPDS card number: 21-1272, tetragonal) without secondary phases, amorphous material or impurities. But, for TiO_2-0.5c and TiO_2-0.5m no peaks were seen. Due to an excess biomolecules of *citrus aurantium* and *musa acuminate* extracts used that leads to amorphous phase TiO_2 NPs [81].

GO diffraction pattern Figure 16 (e and f) showed a broad and relatively strong characteristic peak at 2θ=10.1° corresponding to (0 0 1) plane which indicates that the GO sheets. The spacing between GO sheets was attributed to the presence of oxygen functional groups such as hydroxyl, carboxyl and epoxide groups on the carbon backbones [82]. Also an incomplete oxidation of graphite powder was exhibit a strong and sharp diffraction peak at 26.1° corresponding to (002) plane.

The XRD patterns of TiO_2/rGO-0.5 TiO_2/rGO-1 and TiO_2/rGO-1.5 nanocomposites shown Figure 16(c and d) were similar to TiO_2 NPs peaks position, but low peaks intensity and some impurity were seen due to incomplete oxidation of graphite and the cluster of biomolecules from phytochemical of CA and MA extracts during synthesis method. However, the characteristic diffraction peaks of GO were not found in the XRD pattern of composites due to the low amount used and its reduction during the synthesis process [83].

The average crystal size of all synthesize nanomaterials by CA and MA extracts were calculated by using Debye Scherer's Equation 13, and given in Table 1.

As compared to both *citrus aurantium* and *musa acuminate* extracts synthesis for single and composite nanomaterials similar XRD phase and different intensity results were obtained. This shows the phytochemical composition of each extracts are similar in FTIR results.

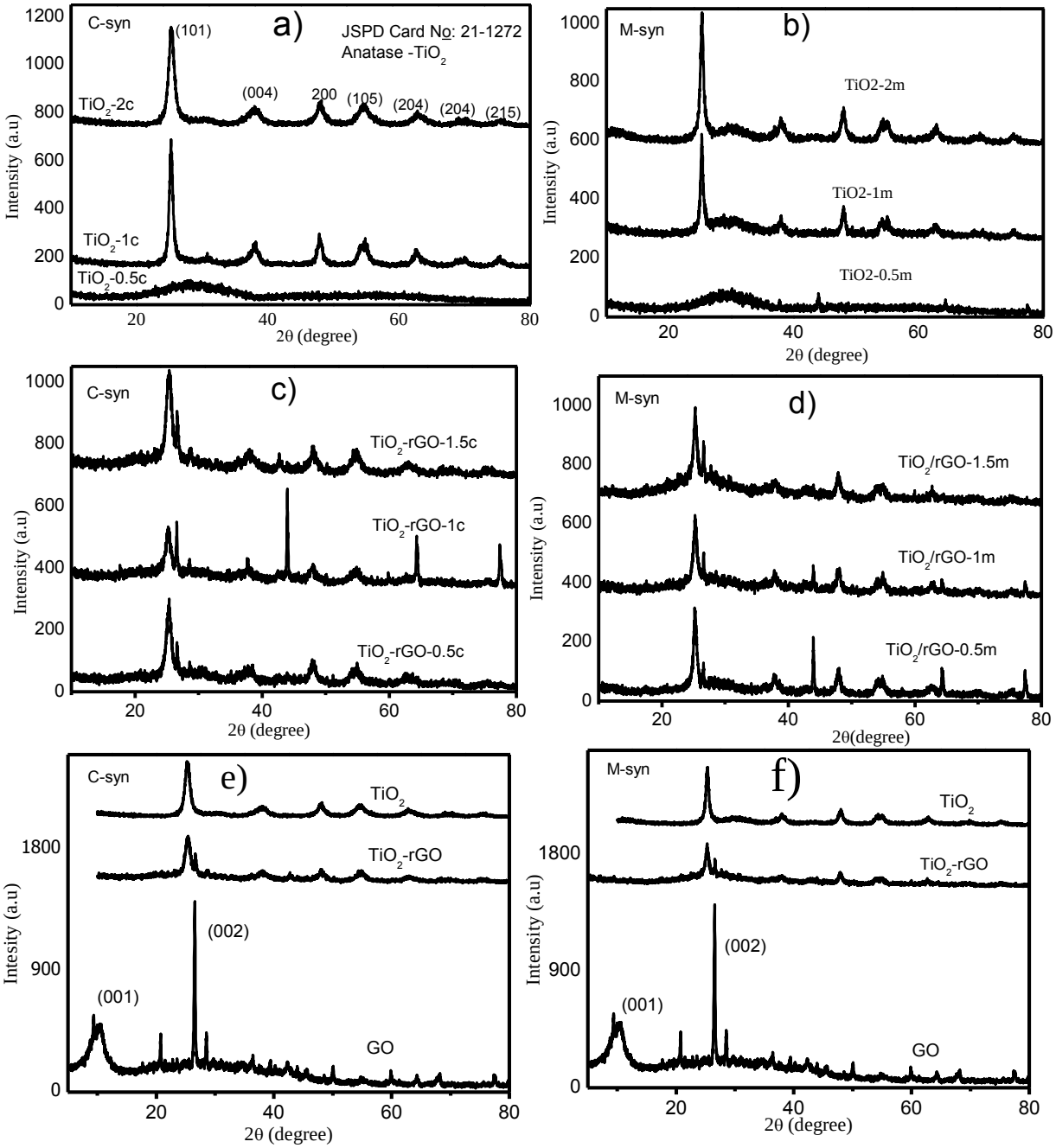

Figure 16. XRD pattern of: TiO_2 NPs (a, b), TiO_2/rGO NCs (c, d), and GO, TiO_2 and TiO_2/rGO (e, f).

Table 1. Calculated crystal size of GO, TiO_2 and TiO_2/rGO nanomaterials.

Nanomaterials	2θ (^{o})	B = FWHM (radian)	Cos θ	βcos θ	D(nm)=kλ/βcosθ k=0.9,λ=0.154
TiO_2-0.5c	27.6	0.01535111	0.33081488	0.00507838	27.29218975
TiO_2-1c	25.3	0.01151333	0.9965051	0.0114731	12.08043647
TiO_2-2c	25.3	0.01918889	0.9965051	0.01912183	7.248261883
TiO_2-0.5m	26.1	0.00697778	0.88531311	0.00617752	22.43619473
TiO_2-1m	25.3	0.00854778	0.9965051	0.0085179	16.27160831
TiO_2-2m	25.4	0.01046667	0.99108487	0.01037335	13.36115462
TiO2/rGO-0.5c	25.07	0.00907111	0.99950798	0.00906665	15.28679623
TiO2/rGO-1c	25.4	0.01657222	0.99108487	0.01642448	8.438623972
TiO2/rGO-1.5c	25.4	0.01866556	0.99108487	0.01849915	7.492236237
TiO2/rGO-0.5m	25.3	0.01116444	0.9965051	0.01112543	12.45795011
TiO2/rGO-1m	25.3	0.01221111	0.9965051	0.01216843	11.39012582
TiO2/rGO-1.5m	25.3	0.01238556	0.9965051	0.01234227	11.22970151
GO	10.1	0.02093333	0.6725218	0.01407812	9.8450624

4.3 FT-IR Analysis

The Fourier transform infrared spectroscopy (FTIR) analysis helps to examine the functional groups and was investigated in the wavenumber ranges of 4000-400 cm^{-1} for CA, MA, GO, TiO_2/rGO and TiO_2 as shown in Figure 17.

GO displayed numerous typical absorption bands corresponds to oxygen functionalities present on GO sheet. The band at 1725 cm^{-1} credited to the C = O (carbonyl) and the wide band around 3000– 3600 cm^{-1} is ascribed to the O–H (hydroxyl) stretching vibrations of the C-OH groups due to moisture absorbed onto the surface of prepared sample. The band corresponds to 1056 cm^{-1} and 1248 cm^{-1} are credited to C-O (carboxylates) and C-O-C (epoxide) stretching modes, respectively. The sp^2 hybridized carbon (C = C) skeleton vibration peak could be seen in GO around 1633 cm^{-1}. Compared to GO, rGO in TiO_2/rGO shows significant reduction in absorption intensities due to oxygen containing functional groups like carboxylates, epoxide, carbonyl indicating the green reduction of GO to rGO by both *citrus aurantium* and *musa acuminate* extracts [78].

FT-IR spectra of TiO_2 showed the broad band below 1000 cm^{-1} which indicates replicate Ti-O-Ti linkage in TiO_2. The TiO_2/rGO exhibited low intensity band frequency compared to GO which is formed by amalgamation of ((Ti-O-Ti) and (Ti-O-C) linkages owing to the chemical interaction of TiO_2 with rGO sheets. The obtained spectra confirmed green reduction of GO and coupling the TiO_2 on the rGO sheets [84].

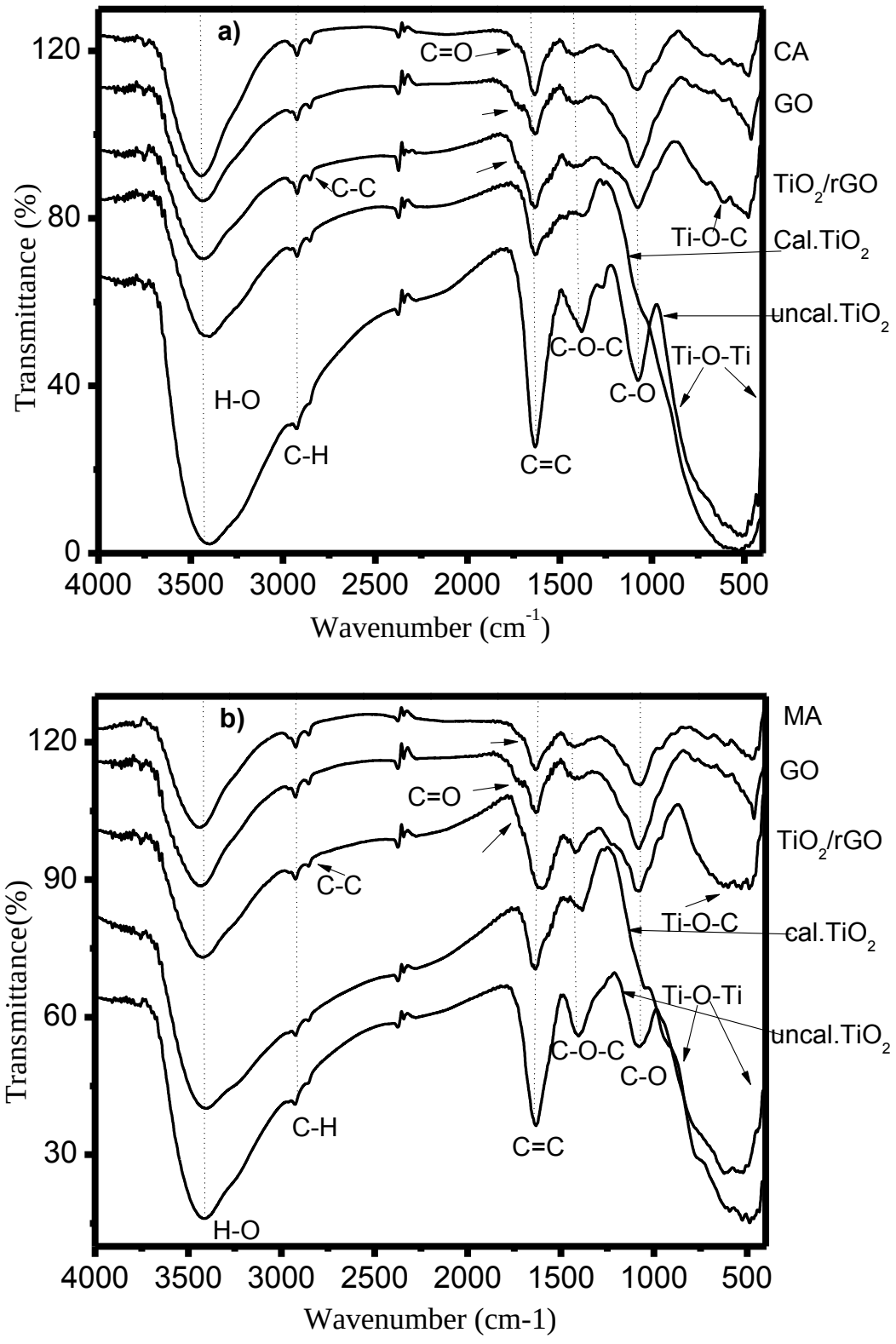

Figure 17. FTIR spectrum of a) CA, GO, TiO_2 (calcined and uncalcined) and TiO_2/rGO synthesized by CA extract, and b) MA, GO, TiO_2 (calcined and uncalcined) and TiO_2/rGO synthesized by MA extract.

4.4 UV-Vis DRS Analysis

The experimental energy band gap for the GO, TiO_2 and TiO_2/rGO synthesized by *citrus aurantium* and *musa acuminate* with different ratios were measured from the Tauc plots graph method. UV-Vis DRS absorption spectroscopy data measurement of percent reflectance versus wavelength graph values were converted to Tauc plots technique and the graphs between Kubelka-Munk function ([F(R (∞) hv] ^1/2 versus Energy (Eg) were drawn in Figure 18 and 19.

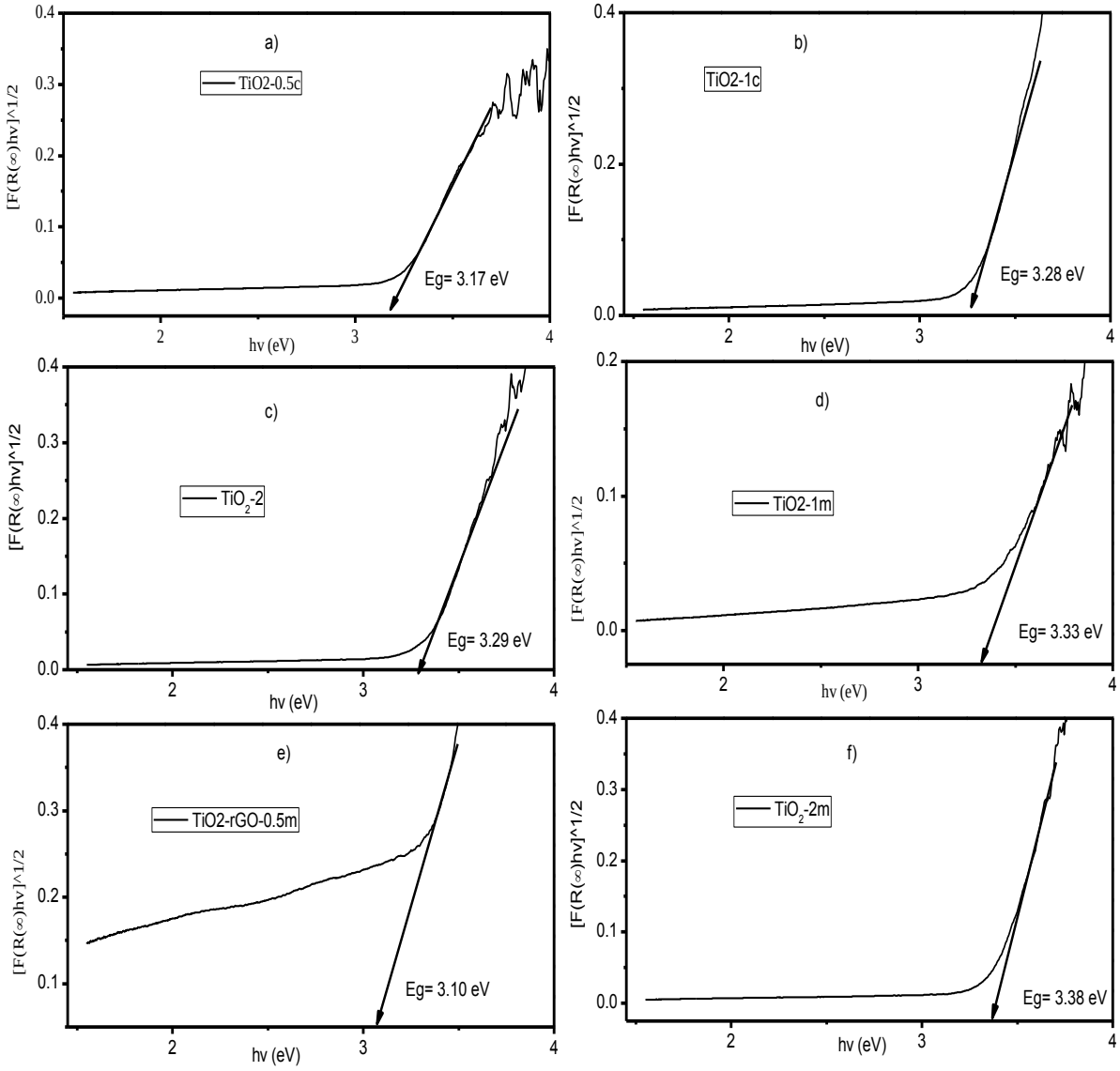

Figure 18 Tauc plot ([F(R (∞) hv] ^1/2 vs hv) for TiO_2 synthesized 0.5, 1 and 1.5 ratios using CA and MA extracts obtained from percent reflectance measurements.

Figure 18 shows energy band gap of TiO_2 nano particles obtained from Tauc plots. The experimental energy band gap of TiO_2-0.5, TiO_2-1 and TiO_2-2 synthesized by *citrus aurantium* and *musa acuminate* were 3.17eV, 3.28 and 3.29 eV, and 3.10, 3.33 and 3.38 eV respectively. The energy will slightly increasing with increasing extract volumes.

As we seen from Figure 19a, the experimental energy band gap for the GO is found to be 1.49 eV. From experimental graph, it is known that the graphene oxide which was produced via chemical exfoliation method have less energy band gap compared to TiO_2 NPs. So, from the reduction process the graphene oxide is reduced through *citrus aurantium* and *musa acuminate* extracts and hence the reduced graphene oxide is formed and coupled with TiO_2 NPs for which the energy band gap is found to be less than energy band gaps of TiO_2 NPs and greater than energy band gap of GO.

Figure 19 (b-g) shows energy band gap of TiO_2/rGO nano composite obtained from Tauc plots. The experimental energy band gap of TiO_2/GO-0.5, TiO_2/GO-1 and TiO_2/GO-1.5 synthesized by *citrus aurantium* and *musa acuminate* were 3.11eV, 3.05 and 2.85 eV, and 3.11, 3.07 and 2.96 eV respectively.

Increasing GO concentrations in the composite tends to decrease energy band gap for both extracts. In the presence of GO influences the optical properties of light absorption significantly. With the addition of GO in the nanocomposites, light absorption intensity in the UV region grows and a red shift to higher wavelength in the absorption edge at about 400 nm is also observed [85]. Increased background in the area 400–800 nm is caused by the incorporation of GO into the matrix of TiO_2.

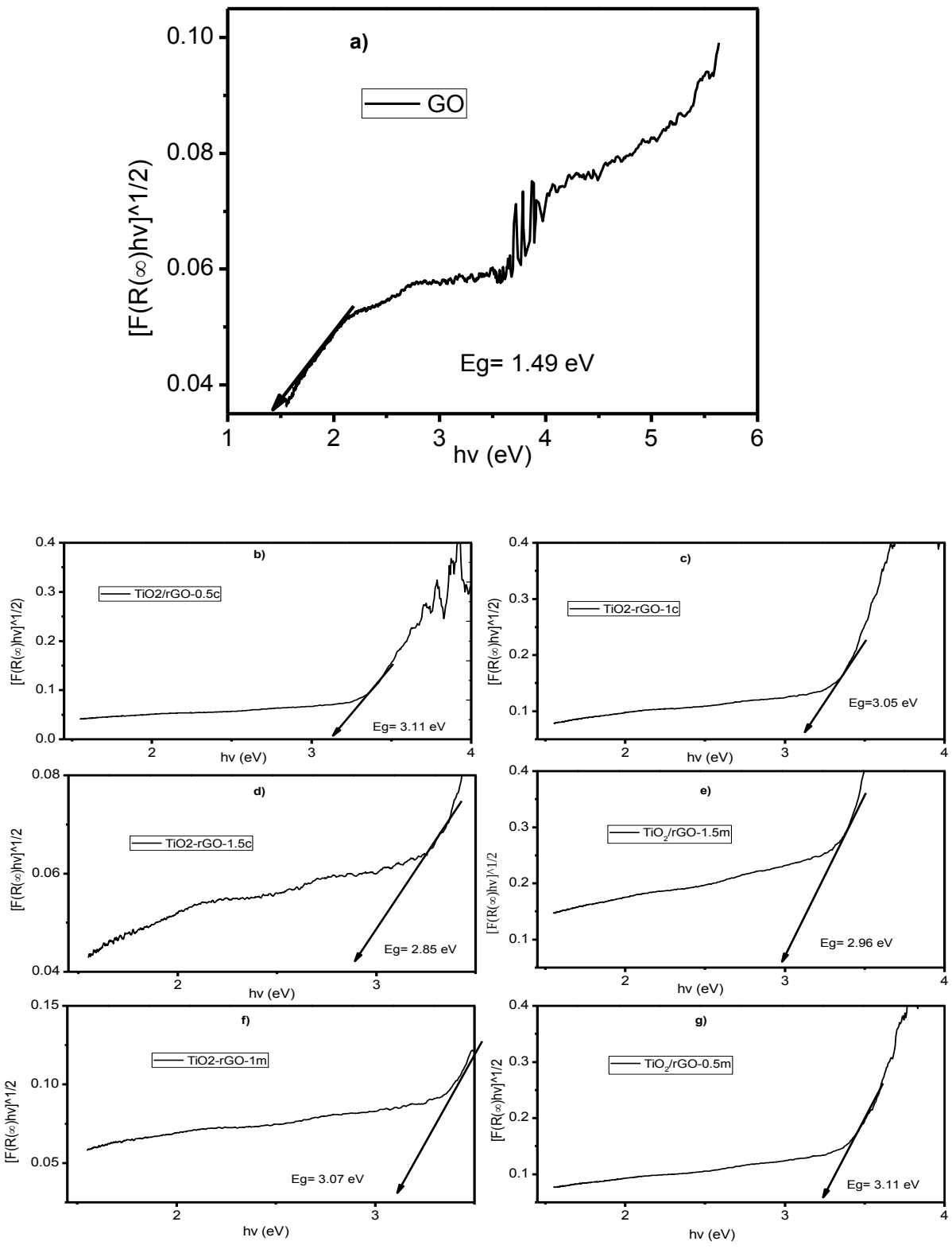

Figure 19.Tauc plot ([F(R (∞) hv] ^1/2 vs hv) for TiO_2/rGO synthesized 0.5, 1 and 1.5 using CA and MA extracts (b-g) and GO (a) obtained from percent reflectance measurements.

4.5 Morphologies of GO, TiO_2 Nanoparticles and TiO_2/rGO Nanocomposite

The typical SEM image of spray-dried GO, TiO_2 nanoparticles and TiO_2/rGO nanocomposite are shown in Figure 20 (a-e). Figure 20e shows reveals the existence of crumple structure for graphene oxide. This is due to the exfoliation of graphite to become graphene oxide and results in deformation upon the exfoliation and restacking. As seen in the image of reduced graphene oxide (rGO), the folded and wrinkled structure has been observed. This folding structure can be found on both surface and the edge of rGO due to the losses of oxygen functional groups. More folded and wrinkled structure is produced when the reduction is stronger [86]. Figure 20 (a, and d) shows a SEM micrograph of TiO_2 nanoparticles prepared by citrus *aurantium* and *musa acuminate* extracts. From the micrograph it is clearly seen that the particles are spherical shape and uniformly distributed. Larger particles in this Figures may be aggregates of the smaller particles. Figure 20 (b and c) shows TiO_2 nanoparticles are distributed uniformly on the surface of rGO particles forming TiO_2/rGO nanocomposite.

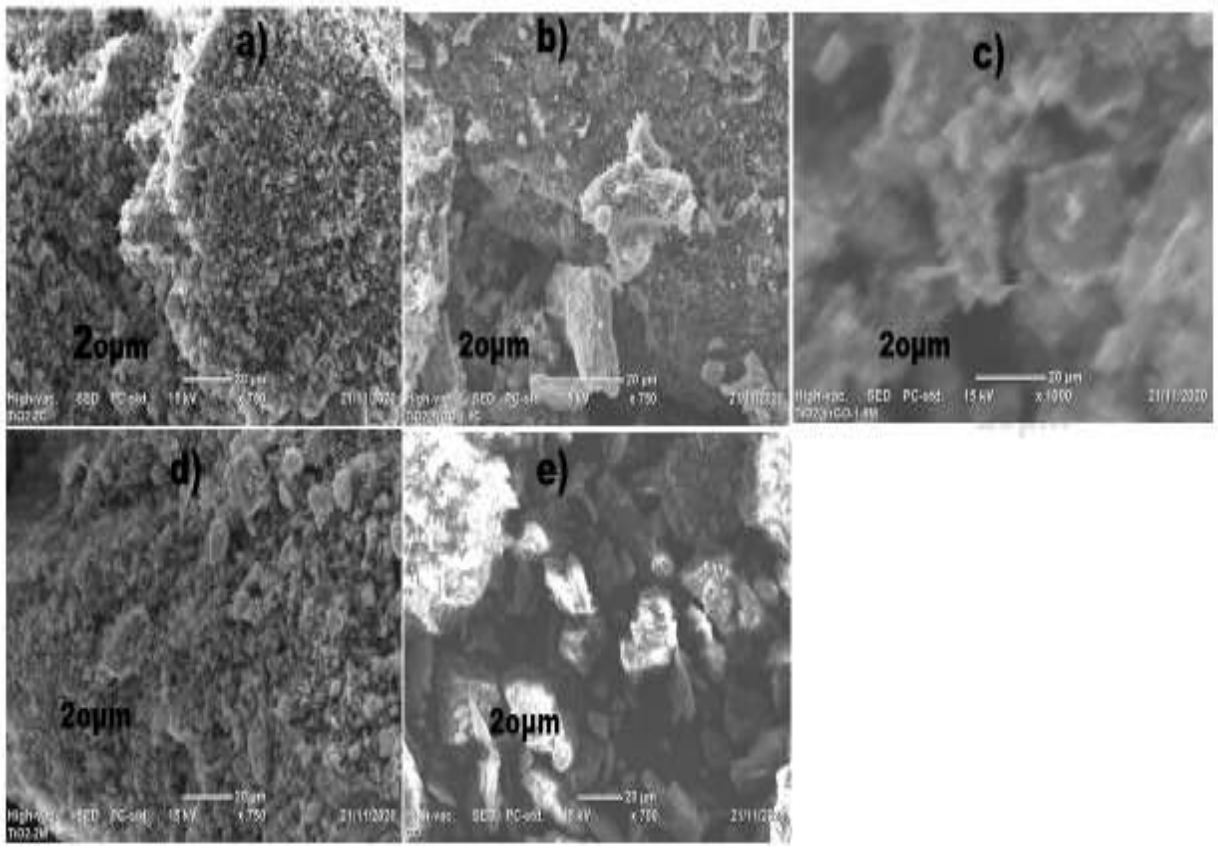

Figure 20. SEM images of different samples, a) TiO_2-2c, b) TiO_2/rGO-1.5c, c) TiO_2/rGO-1.5m. d) TiO_2-2m, and e) GO.

4.6 Photocatalytic Performance of TiO_2 Nanoparticle and TiO_2/rGO NC

In Figure 21 (a, and e) shows the absorbance of methylene blue photocatalytic degradation after 60 minute by TiO_2 nanoparticles and Figure 21 (b-d and f-h) shows TiO_2/rGO nanocomposites with different concentrations synthesized by both CA and MA extracts. As we seen from the graph, intensity of single oxides (TiO_2-2c and TiO_2-2m) were high this indicates less degradation of MB. But when composites of different ratios TiO_2/rGO-0.5c, TiO_2/rGO-1c and TiO_2/rGO-1.5c, and TiO_2/rGO-0.5m, TiO_2/rGO-1m and TiO_2/rGO-1.5m

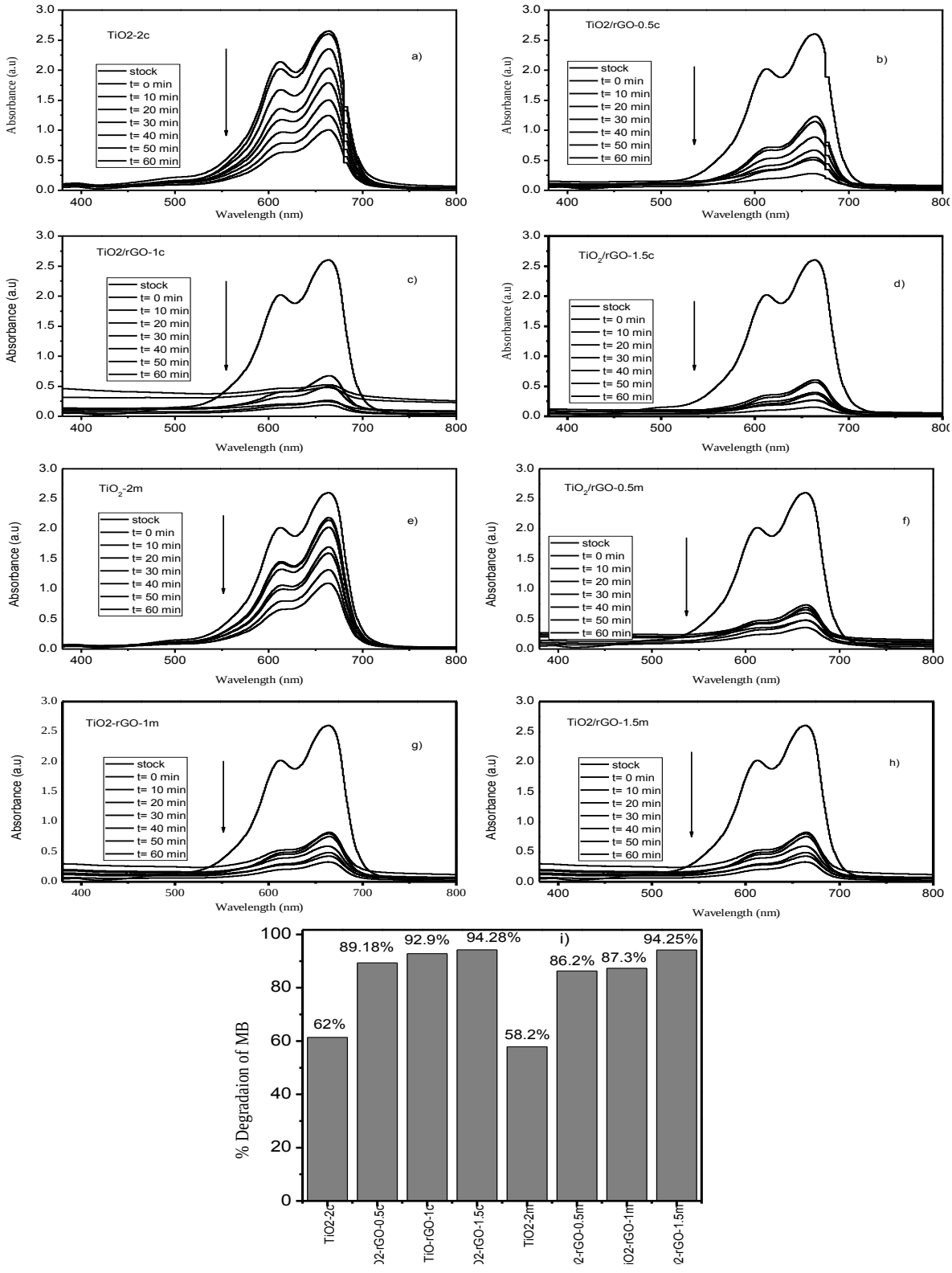

Figure 21. The absorbance of MB after illumination of light for 60 minutes in the presence of TiO_2 and TiO_2/rGO catalysts synthesized by CA and MA extracts, and photocatalytic degradation efficiency.

were used, the absorbance were highly decreased with irrespective increasing ratios of composites, which implies high degradation of methylene blue. Figure 21i shows percent photocatalytic degradation of methylene blue. TiO_2/rGO-1.5c and TiO_2/rGO-1.5m shows slightly difference photocatalytic degradation efficiency of MB (94.28%) and (94.25%) respectively within 60 minutes with illumination of halogen lamp.

The photocatalytic degradation of methylene blue by using TiO_2 and TiO_2/rGO nanocomposite synthesized by *citrus aurantium* and *musa acuminate* were given in Figure 22. A reaction kinetics study model for photocatalytic degradation of methylene blue in the presence of halogen lamp illumination with either TiO_2 or TiO_2/rGO catalysts synthesized by both extracts were tested by using first and second order of pseudo kinetic model. As compared from Figure 22 (a, and b) , it is seen that photocatalytic degradation of methylene blue fit pseudo first order model as the correlation constant for the fitted line to be $R^2 > 0.95$. Good correlation to first order reaction kinetics ($R^2 = 0.95$ for TiO_2-2c and $R^2 = 0.953$ for TiO_2-m) for single oxide were found. But for composites were didn't fit pseudo first order model. For pseudo second order kinetic model good correlation constant was only $R^2 = 0.974$ for TiO_2/rGO-1.5m, others didn't fit $R^2 > 0.95$. Therefore photocatalytic degradation of methylene blue is pseudo first order reaction with respect to TiO_2 nanoparticles and pseudo second order reaction with respect TiO_2/rGO nanocomposites synthesized by *citrus aurantium* and *musa acuminate* extracts.

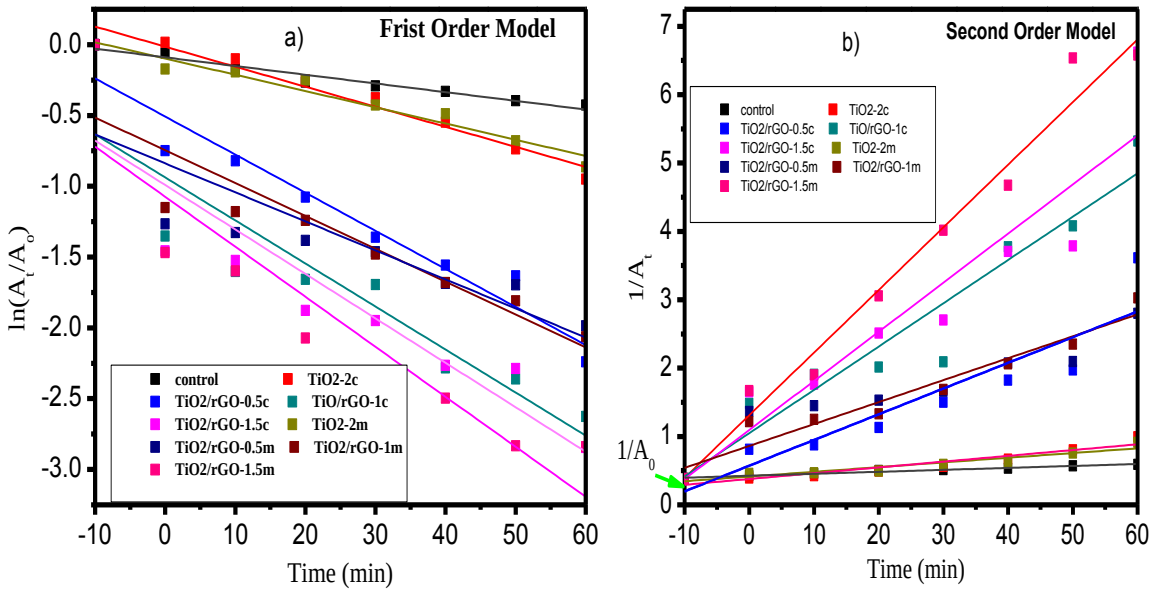

Figure 22. Frist and second order kinetic model for photocatalytic degradation of MB.

Table 2. Calculated first and second order kinetic data model.

First order ($\ln(A_t/A_i)= -kt$) data				**Second order ($1/A_t= kt + 1/A_o$) data**			
Nanomaterials	**Intercept**	**slope**	**R^2**	**Nanomaterials**	**Intercept**	**slope**	**R^2**
Control	-0.098	-0.006	0.955	control	0.42581	0.00287	0.9802
TiO_2-2c	-0.01	-0.014	0.95	TiO_2-2c	0.37816	0.00846	0.88616
TiO_2/rGO-0.5c	-0.051	-0.024	0.83	TiO_2/rGO-0.5c	1.09519	0.07185	0.85933
TiO_2/rGO-1c	-0.94	-0.03	0.8	TiO_2/rGO-1c	1.04936	0.06333	0.85933
TiO_2/rGO-1.5c	-1.07	-0.036	0.828	TiO_2/rGO-1.5c	1.09519	0.07185	0.85933
TiO_2-2m	-0.098	-0.011	0.953	TiO_2-2m	0.41428	0.00688	0.8976
TiO_2/rGO-0.5m	-0.084	-0.02	0.66	TiO_2/rGO-0.5m	0.5731	0.03761	0.81955
TiO_2/rGO-1m	-0.75	-0.02	0.79	TiO_2/rGO-1m	0.8615	0.03209	0.92895
TiO_2/rGO-1.5m	-1.07	-0.035	0.819	TiO_2/rGO-1.5m	1.31106	0.09163	0.97396

4.6.1 Effect of pH

The influence initial pH of the solution on the degradation efficiency of methylene blue was investigated at pH 1, 7, and 13 as shown in Figure 23. The change in the pH of the solution influences the surface of the catalyst, thereby causing a change in adsorption and reaction rate [87]. The point of zero charges of the TiO_2/rGO-1.5c was estimated to be at pH 7. Therefore, the catalyst surface will have a negative charge at pH > 7, and a positive charge at pH < 7. It was observed that maximum degradation of MB occurred at pH 7 and minimum at pH 1. When the initial pH increased from 1 to 7, the degradation efficiency increased from 18.1 % to 90.7 %. A further increase in pH from 7 to 13 led to the increase in the degradation efficiency from 90.7 % to 99.4 %. The main reason for the dropped degradation efficiency at pH 1 is due to the electrostatic repulsion between the positively charged catalyst surface and the cationic methylene blue, while no such repulsion would occur at pH 7. Although the adsorption was highest at pH 13 indicating that alkaline pH favored the adsorption due to the electrostatic attraction between negatively charged catalyst surface and cationic methylene blue dye [88], the degradation was negatively affected. This was further investigated, and was observed due to the adverse effect of the alkaline pH on the rGO thus affecting the photocatalytic activity of the sensitized catalyst (supplementary information). Hence, the optimum pH was fixed at pH 7 for further experiments.

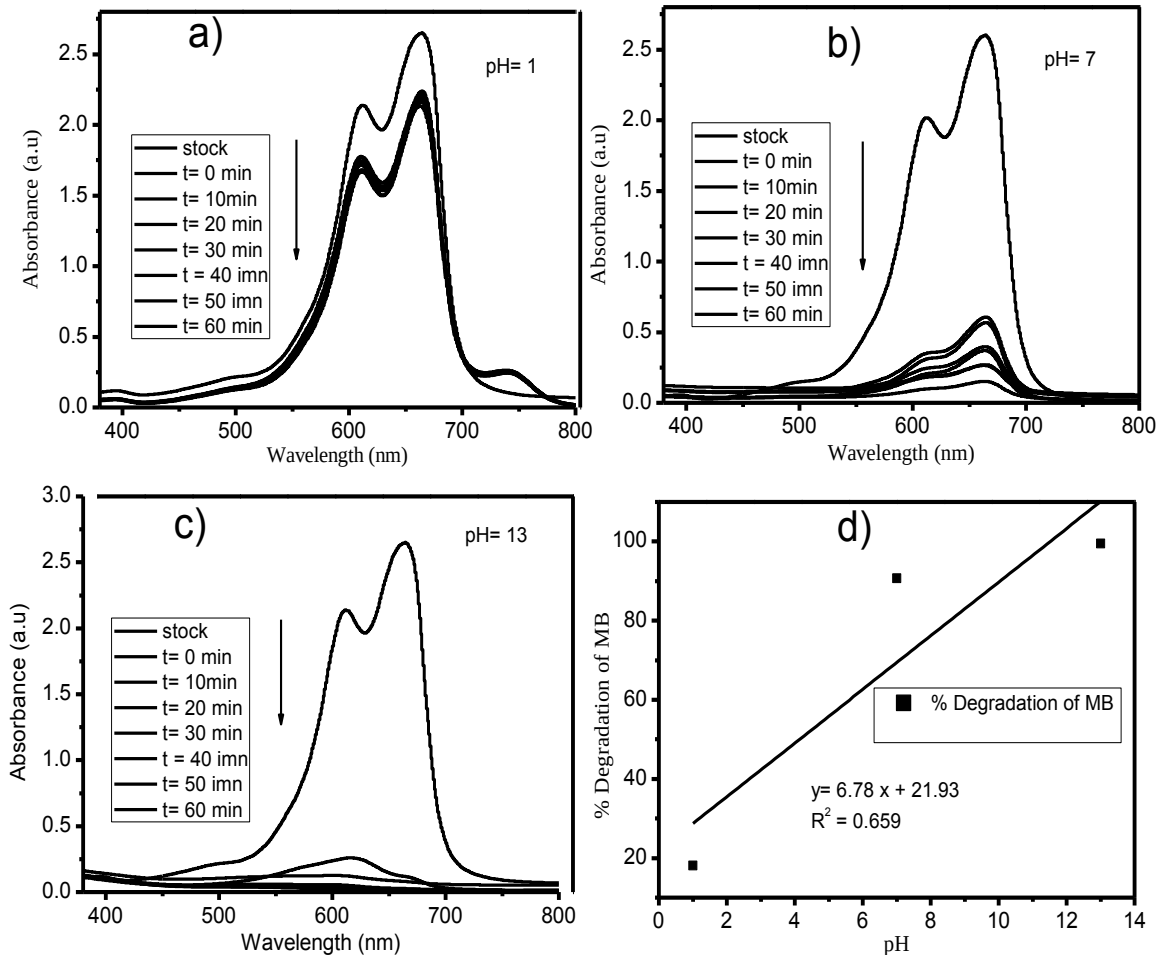

Figure 23. The effect of pH on photocatalytic degradation of MB using TiO_2/rGO-1.5 catalyst synthesized by CA.

4.6.2 Effect of contact time

The effect of visible light illumination contact time from 10 to 60 min was carried out in standard 20 mg/l aqueous solution of MB dye at pH value of 7 and catalyst amount of 30 mg. The reaction started at dark condition for 10 minutes to attain sorption-desorption equilibrium between the catalytic surface and the dye. Figure 24 showed that a noticeable gradual increase of photocatalytic rate with increasing illumination time. After 60 min, the rate reached its maximum removal 94.4%. The results revealed a linear relationship between degradation of MB dye with contact time increasing which explained on the basis of increasing time more and more light energy falls on the catalyst surfaces which induced formation of photon excited species and enhances the photocatalytic activities [87].

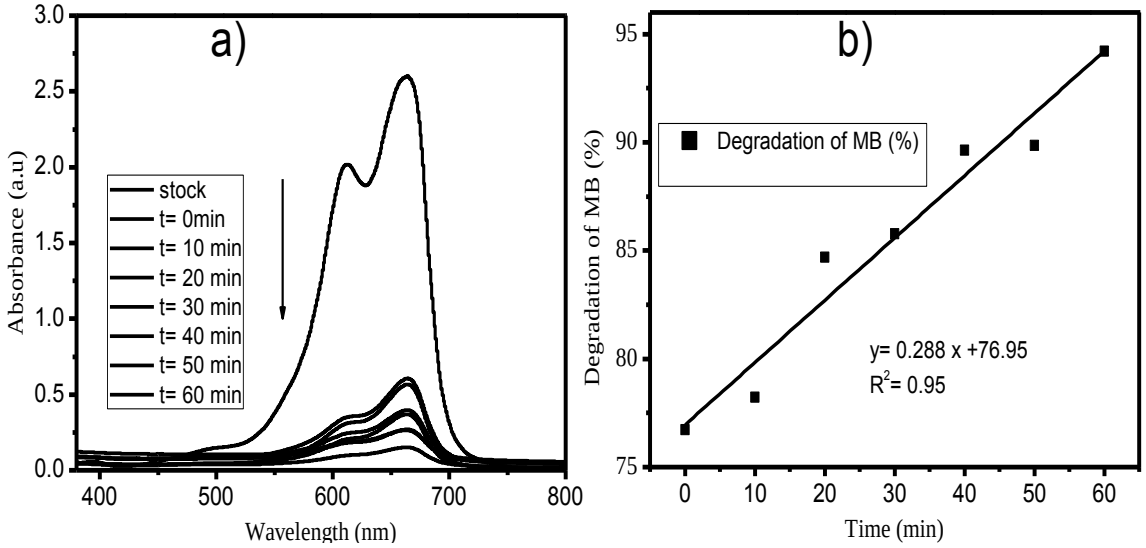

Figure 24. The effect of time on photocatalytic degradation of MB by TiO_2/rGO-1.5 catalyst synthesized by CA.

4.6.3 Effect of Initial Dye Concentration

The initial MB concentrations were 10 mg/l, 20 mg/l and 30 mg/l at catalyst dosage of 30 mg and initial pH 7 used during the photocatalytic experiments. In Figure 25 (a-c), it is clear that as the concentration of MB increased, the degradation efficiency decreased due to the interference for visible light to penetrate and reach the catalyst surface, thereby lowering the production of $^{\cdot}OH$ radicals. In addition, with higher MB concentration, the produced $^{\cdot}OH$ radicals might be insufficient due to increasing demand. The concentration of intermediates formed would also be higher with increased MB concentrations inducing a competition for $^{\cdot}OH$ radical reaction with MB, and thereby lowering the rate of MB degradation [88] . The reaction rates were found to decrease with increasing MB concentration from the rate constant of 0.04 min^{-1} for 10 mg/l to 0.02 min^{-1} for 30 mg/l and followed the pseudo first order kinetic model (see Figure 23d).

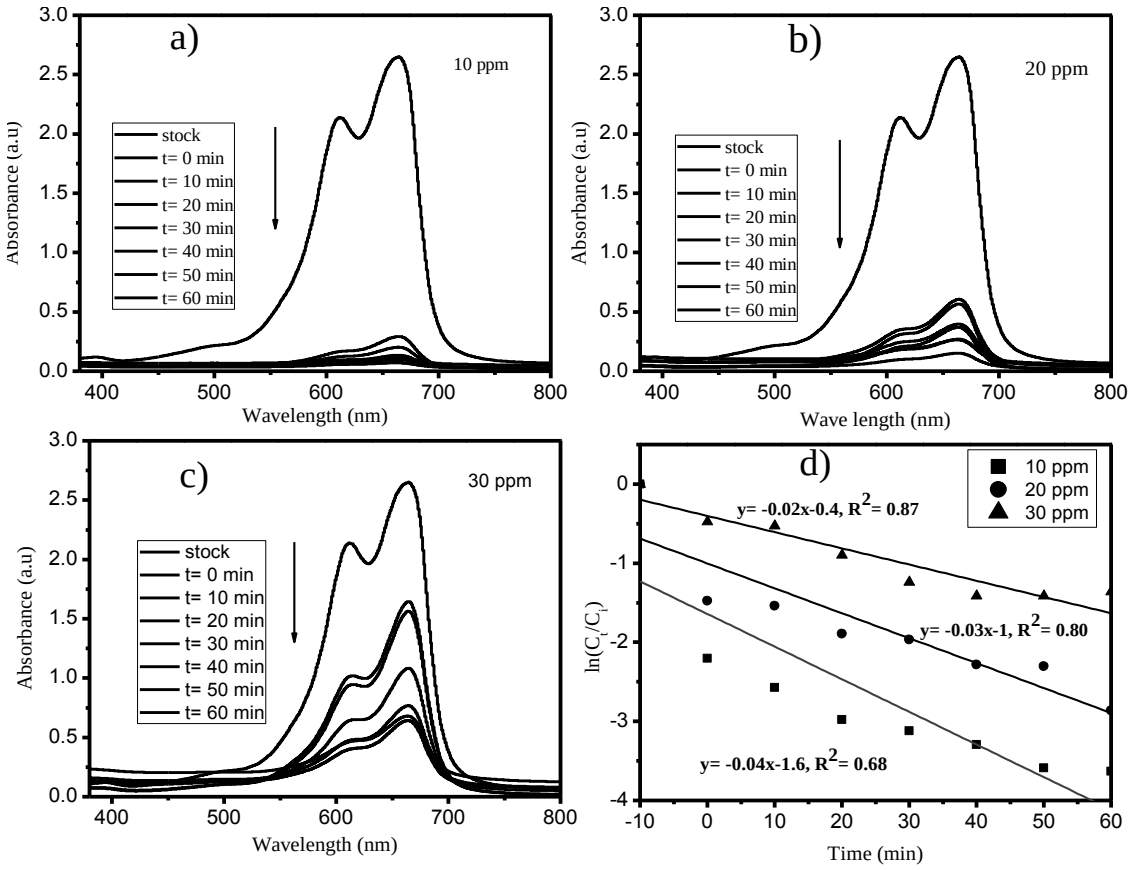

Figure 25. The effect of initial concentration on photocatalytic degradation of MB using TiO_2/rGO-1.5 catalyst synthesized by CA.

4.6.4 Effect of Catalyst Dosage:

Degradation experiments were conducted at initial pH of 7 and initial MB concentration of 20 mg/l by varying the catalyst dose of 10, 30 and 50 mg (Figure 26). An increase in the degradation efficiency was observed with the increase in catalyst dosage. The increase in catalyst dosage increases the total number of active sites on the catalyst surface thereby producing more OH radicals that can take part in the degradation of dye [37]. The maximum degradation efficiency of 90.92 % was obtained with 50 mg of catalyst dosage. However, considering the economic feasibility, the optimum catalyst dosage was selected as 30 mg since it could also achieve a sufficiently high degradation efficiency (~90.70%), and also since almost doubling the catalyst concentration to 50 mg resulted in only ~0.24 % increase in the overall efficiency.

In general due to increasing in active sites, the rate of photocatalytic degradation organic pollutants increases with photocatalyst dosage. At lower catalyst loading, degradation of organic molecule is low, because more light is transmitted through the reactor and lesser

transmitted radiation only will be utilized in the photocatalytic reaction. But beyond the optimum amount of catalyst loading, the degradation rate might be reduced due to increase in the opacity of the suspension, and thus increasing the light scattering and also the infiltration depth of the photons is diminished and less photocatalyst could be activated. Additional to what is mentioned above, agglomeration of nanoparticles at high concentrations reasoning a decline in the number of surface active sites available for the photocatalytic degradation and deactivation of activated molecules could result from the collision of activated molecules with ground state molecules [39].

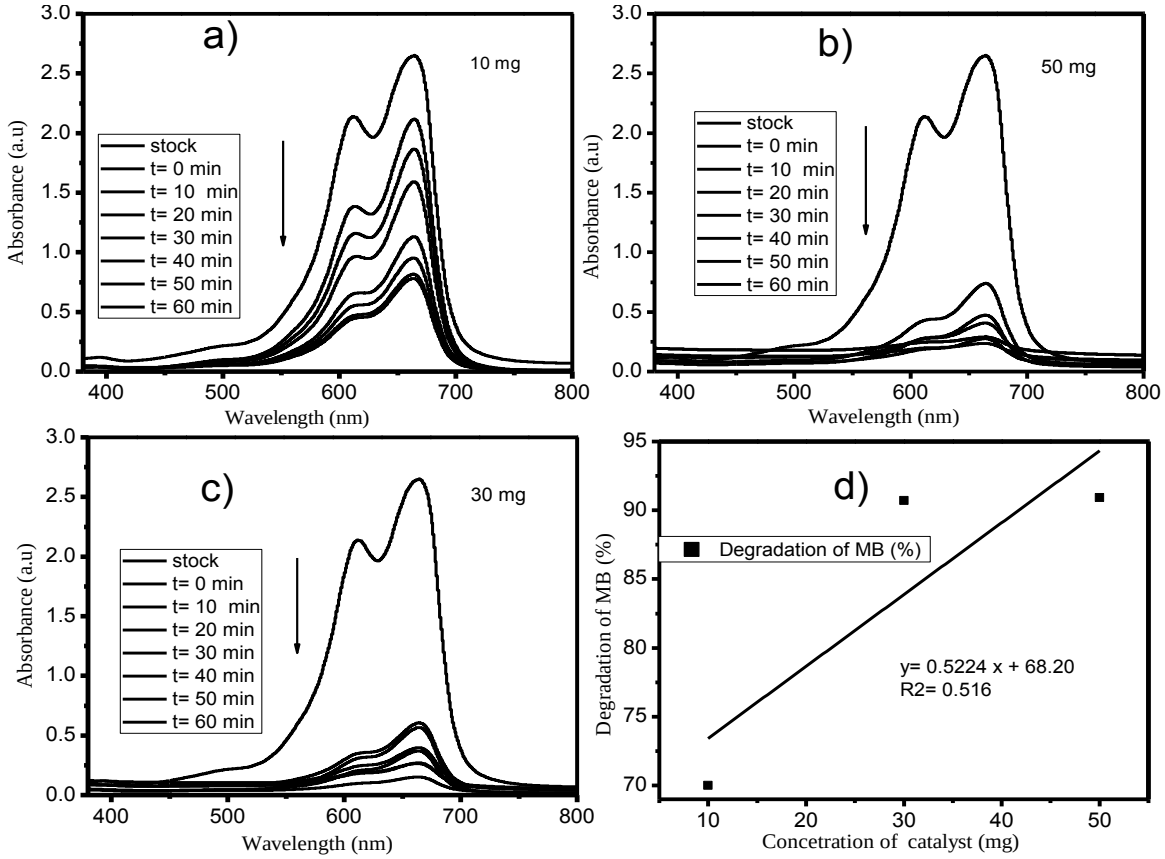

Figure 26. The effect of catalyst dosage on photodegradation of MB by TiO_2/rGO-1.5 catalyst synthesized by CA.

5. CONCLUSION AND RECOMMENDATION

5.1 Conclusion

TiO_2-rGO NC was effectively synthesized by MA and CA as a green reducing, stabilizing and capping agent via co-precipitation technique. XRD and FT-IR studies were confirmed the phyoreduction of GO to rGO, TiO_2 and formation of TiO_2/rGO NC by MA and CA. The DRS showed that the formation of TiO_2 on graphene surface had promoted the absorption in visible area. Microball-like morphology of TiO_2 anchored on the surface of rGO sheets was shown by the SEM images. TiO_2/rGO (94.28%) nanocomposites show good photocatalytic activity toward the degradation of MB dye under illumination of halogen lamp (150W) than TiO_2 (58.2%) single NPs. The photocatalytic activity increases when the surface of TiO_2 is modified by increasing amount of GO. The best catalytic activity is observed with TiO_2/rGO-1.5 synthesized by *citrus aurantium* and *musa acuminate* extracts, resulting in 94.28 % and 94.25% MB degradation respectively after 60 min under visible light. This shows the phytochemical composition of *citrus aurantium* and *musa acuminate* extracts are similar as confirmed from FTIR results only intensity difference. As using first and second order kinetic model photocatalytic degradation of methylene blue was fit pseudo first order reaction with respect to TiO_2 nanoparticles and pseudo second order reaction respect to TiO_2/rGO nanocomposite. Also the dependences of photocatalytic degradation of methylene blue were investigated under changes of pH, catalyst dosage, reaction time, and initial concentration of pollutants. Catalytic dosage, pH and reaction time have positive effects whereas initial concentration of pollutant has negative effect at optimum conditions.

5.2 Recommendations

Based on the present findings, TiO_2/rGO nanocomposite could be synthesized by *Citrus aurantium* and *musa acuminate* extracts. Those materials were environmental waste but useful for synthesis as reducing and capping agents. Therefore, using waste as raw materials add values for environmental cleans. The surfaces of TiO_2/rGO NC highly adsorb the pollutants. Also it is difficult to write the mechanism of photocatalytic degradation activity of methylene blue. Therefore NMR study should be conducted to write structural elucidation mechanism and adsorption efficiency should be studied.

6. REFERENCE

1. Kumar, R.,Graphene/metal oxide–based nanocomposite as photocatalyst for degradation of water pollutants. 2019: **1**(1): p. 1-20.
2. Bhanvase, B.A., T.P. Shende, and S.H. Sonawane, A review on graphene–TiO_2 and doped graphene–TiO_2 nanocomposite photocatalyst for water and wastewater treatment. Environmental Technology Reviews, 2016. **6**(1): p. 1-14.
3. Wu, T., Dye Degrading and Fouling-Resistant Membranes Formed by Deposition with Ternary Nanocomposites of N-Doped Graphene/TiO_2/Activated Carbon. Membranes (Basel), 2019. **9**(1): p.1-9.
4. Akhila, A.K., P.S. Vinitha, and N.K. Renuka, Photocatalytic Activity of Graphene – Titania Nanocomposite. Materials Today: Proceedings, 2018. **5**(8): p. 1-16.
5. Sher Shah, M.S.,Green synthesis of biphasic TiO_2-reduced graphene oxide nanocomposites with highly enhanced photocatalytic activity. ACS Appl Mater Interfaces, 2012. **4**(8): p. 1-19.
6. K, S.S., Green Synthesis of High Temperature Stable Anatase Titanium Dioxide Nanoparticles Using Gum Kondagogu: Characterization and Solar Driven Photocatalytic Degradation of Organic Dye. Nanomaterials (Basel), 2018. **8**(12): p. 1-15.
7. John, D., TiO_2-reduced graphene oxide nanocomposites for the trace removal of diclofenac. SN Applied Sciences, 2020. **2**(5): p. 1-17.
8. Kulkarni, P., Conventional wastewater treatment and reuse site practices modify bacterial community structure but do not eliminate some opportunistic pathogens in reclaimed water. Sci Total Environ, 2018. **6(1)**: p. 1-11.
9. Nayeri, D. and S.A. Mousavi, Dye removal from water and wastewater by nanosized metal oxides - modified activated carbon: a review on recent researches. Journal of Environmental Health Science and Engineering, 2020. **1**(1: p. 1-30.)
10. Elshahawy, M.F., Fabrication of TiO_2 Reduced Graphene Oxide Based Nanocomposites for Effective of Photocatalytic Decolorization of Dye Effluent. Journal of Inorganic and Organometallic Polymers and Materials, 2020. **30**(7): p. 1-35.
11. Kurniawan, T.A., Functionalizing TiO_2 with graphene oxide for enhancing photocatalytic degradation of methylene blue (MB) in contaminated wastewater. Journal of Environmental Management, 2020. **270**(1): p. 1-18.

12. Nasrollahzadeh, M., An Introduction to Nanotechnology. 2019. **28**(1): p. 1-27.
13. Hong, N.H., Introduction to Nanomaterials: Basic Properties, Synthesis, and Characterization. 2019. **1**(1): p. 1-19.
14. Khan, I., K. Saeed, and I. Khan, Nanoparticles: Properties, applications and toxicities. Arabian Journal of Chemistry, 2019. **12**(7): p. 1-19.
15. Anu Mary Ealia, S. and M.P. Saravanakumar, A review on the classification, characterisation, synthesis of nanoparticles and their application. IOP Conference Series: Materials Science and Engineering, 2017. **263**(1**)**: p. 1-29.
16. Nasir, S., Carbon-Based Nanomaterials/Allotropes: A Glimpse of Their Synthesis, Properties and Some Applications. Materials, 2018. **11**(2): p. 1-15.
17. Vinci, G. and M. Rapa, Noble Metal Nanoparticles Applications: Recent Trends in Food Control. Bioengineering, 2019. **6**(1): p. 1-12.
18. Adireddy, S., Polymer-ceramic nanocomposites for high energy density applications. Journal of Sol-Gel Science and Technology, 2014. **73**(3): p. 1-16.
19. Biju, V., Semiconductor quantum dots and metal nanoparticles: syntheses, optical properties, and biological applications. Anal Bioanal Chem, 2008. **391**(7): p. 1-20.
20. Derakhshankhah, H., Conducting polymer-based electrically conductive adhesive materials: design, fabrication, properties, and applications. Journal of Materials Science: Materials in Electronics, 2020. **31**(14): p. 1-19.
21. Kaliva, M., Biodegradable Chitosan-graft-Poly(l-lactide) Copolymers For Bone Tissue Engineering. Polymers (Basel), 2020. **12**(2): p. 1-13.
22. Saleh, T.A., Nanomaterials: Classification, properties, and environmental toxicities. Environmental Technology & Innovation, 2020. **20**(1): p. 1-17.
23. Waghmode, M.S., Studies on the titanium dioxide nanoparticles: biosynthesis, applications and remediation. SN Applied Sciences, 2019. **1**(4): p. 1-14.
24. Pawar, M., S. Topcu Sendoğdular, and P. Gouma, A Brief Overview of TiO_2 Photocatalyst for Organic Dye Remediation: Case Study of Reaction Mechanisms Involved in Ce-TiO_2 Photocatalysts System. Journal of Nanomaterials, 2018. **20**(1): p. 1-13.
25. Sabri, M.A., Selection of Suitable Biological Method for the Synthesis of Silver Nanoparticles. Nanomaterials and Nanotechnology, 2016. **6**(1): p. 1-9.
26. Rastogi, A., Biological synthesis of nanoparticles: an environmentally benign approach. 2018. **1**(1): p. 1-21.

27. Singh, J., Green' synthesis of metals and their oxide nanoparticles: applications for environmental remediation. J Nanobiotechnology, 2018. **16**(1): p. 1-18.
28. Pushpamalini, T.,Comparative analysis of green synthesis of TiO_2 NPs using four different leaf extract. Journal of Materials Today Proceedings 2020. **1**(1): p. 1-5.
29. Kirthi, A.V., Biosynthesis of titanium dioxide nanoparticles using bacterium Bacillus subtilis. Materials Letters, 2011. **65**(18): p. 1-27.
30. Rajakumar, G., Fungus-mediated biosynthesis and characterization of TiO_2 nanoparticles and their activity against pathogenic bacteria. Spectrochim Acta A Mol Biomol Spectrosc, 2012. **91**(1**)**: p. 1-9.
31. Singh, V. and S. Negi, Algae: A potential source for nanoparticle synthesis. Journal of Applied and Natural Science, 2018. **10**(4): p. 1-11.
32. Swathi, N., Green synthesis of titanium dioxide nanoparticles using Cassia fistula and its antibacterial activity. International Journal of Research in Pharmaceutical Sciences, 2019. **10**(2): p. 1-16.
33. Pushpamalini, T., Comparative analysis of green synthesis of TiO_2 nanoparticles using four different leaf extract. Materials Today: Proceedings, 2020. **1**(1): p. 1-12.
34. Singh, A., Structural, morphological, optical and photocatalytic properties of green synthesized TiO_2 NPs. Current Research in Green and Sustainable Chemistry, 2020. **3**(1): p. 1-33.
35. Hussain, M., Synthesis, characterization, and photocatalytic application of novel TiO_2 nanoparticles. Chemical Engineering Journal, 2010. **157**(1): p. 1-51.
36. Saravanan, R., F. Gracia, and A. Stephen, Basic Principles, Mechanism, and Challenges of Photocatalysis. 2017. **1**(1): p. 1-20.
37. Krishnan, S. and A. Shriwastav, Application of TiO_2 NPs sensitized with natural chlorophyll pigments as catalyst for visible light photocatalytic degradation of methyl blue. Journal of Environmental Chemical Engineering, 2020. **1**(1): p. 1-19.
38. Zahra, Z., Exposure Route of TiO_2 NPs from Industrial Applications to Wastewater Treatment and Their Impacts on the Agro-Environment. Nanomaterials (Basel), 2020. **10**(8): p. 1-17.
39. Chen, D., Photocatalytic degradation of organic pollutants using TiO_2-based photocatalysts: A review. Journal of Cleaner Production, 2020. **268**(1): p. 1-17.
40. May-Masnou, A., Fast and Simple Microwave Synthesis of TiO_2/Au NPs for Gas-Phase Photocatalytic Hydrogen Generation. Front Chem, 2018. **6**(1): p.1-10.

41. Pellegrino, F., Influence of agglomeration and aggregation on the photocatalytic activity of TiO_2 NPs Applied Catalysis B: Environmental, 2017. **21**(6): p. 1-26.
42. Azeez, F., The effect of surface charge on photocatalytic degradation of methylene blue dye using chargeable titania nanoparticles. Sci Rep, 2018. **8**(1): p. 1-18.
43. Abdellah,M.H.,Photocatalytic decolorization of methyl blue using TiO_2/UV system enhanced by air sparging. Alexandria Engineering Journal, 2018. **57**(4): p.1-15.
44. Kumar, A., A Review on the Factors Affecting the Photocatalytic Degradation of Hazardous Materials. Material Science & Engineering International Journal, 2017. **1**(3): p. 1-22.
45. Ismael, M., A review and recent advances in solar-to-hydrogen energy conversion based on photocatalytic water splitting over doped-TiO_2 nanoparticles. Solar Energy, 2020. **211**(1): p. 1-16.
46. Abed, J., Recent Advances in the Design of Plasmonic Au/TiO_2 Nanostructures for Enhanced Photocatalytic Water Splitting. Nanomaterials, 2020. **10**(11): p. 1-20.
47. Jafari, T., Photocatalytic Water Splitting-The Untamed Dream: A Review of Recent Advances. Molecules, 2016. **21**(7): p. 1-13.
48. Basavarajappa, P.S., Recent progress in metal-doped TiO_2, non-metal doped/codoped TiO_2 and TiO_2 nanostructured hybrids for enhanced photocatalysis. International Journal of Hydrogen Energy, 2020. **45**(13): p. 1-18.
49. Patil, S.B., Recent advances in non-metals-doped TiO_2 nanostructured photocatalysts for visible-light driven hydrogen production, CO_2 reduction and air purification. International Journal of Hydrogen Energy, 2019. **44**(26): p. 1-22.
50. Ansari, S.A., Nitrogen-doped titanium dioxide (N-doped TiO_2) for visible light photocatalysis. New Journal of Chemistry, 2016. **40**(4): p. 1-30.
51. Khokhar, D., Functionalization of conducting polymers and their applications in optoelectronics. Polymer-Plastics Technology and Materials, 2020. **1**(1): p. 1-23.
52. Mondal, A. and N.R. Jana, Graphene-Nanoparticle Composites and Their Applications in Energy, Environmental and Biomedical Science. Reviews in Nanoscience and Nanotechnology, 2014. **3**(3): p. 1-19.
53. Hu, M., Z. Yao, and X. Wang, Characterization techniques for graphene-based materials in catalysis. AIMS Materials Science, 2017. **4**(3): p. 1-17.
54. Smith, B.R., Why believe? The promise of research on the role of religion in entrepreneurial action. Journal of Business Venturing Insights, 2019. **11**(1): p.1-14.

55. Zou, Y., Ultraviolet Detectors Based on Wide Bandgap Semiconductor Nanowire: A Review. Sensors (Basel), 2018. **18**(7): p. 1-15.
56. White, D.L., Synthesis of Holey Graphene Nanoparticle Compounds. ACS Appl Mater Interfaces, 2020. **12**(32): p. 1-22.
57. Coroş, M., A brief overview on synthesis and applications of graphene and graphene-based nanomaterials. Frontiers of Materials Science, 2019. **13**(1): p. 1-32.
58. Atta, N.F., A. Galal, and E.H. El-Ads, Graphene A Platform for Sensor and Biosensor Applications. 2015. **1**(1): p. 1-11.
59. Camargo, P.H.C., K.G. Satyanarayana, and F. Wypych, Nanocomposites: synthesis, structure, properties and new application opportunities. Materials Research, 2009. **12**(1): p. 1-39.
60. Zhao, W., Mechanical properties of nanocomposites reinforced by carbon nanotube sponges. Journal of Materiomics, 2018. **4**(2): p. 1-16.
61. Lucie Bacakova and Julia Pajorova brief review on Application of Nanocellulose/Nanocarbon Composites: Focus on Biotechnolgy and Medicine. Nanomaterials MDPI, 2020. **1**(1): p. 1-34
62. Surmenev, R.A., Hybrid lead-free polymer-based nanocomposites with improved piezoelectric response for biomedical energy-harvesting applications: A review. Nano Energy, 2019. **62**(1): p. 1-26.
63. Omanović-Mikličanin, E., Nanocomposites: a brief review. Health and Technology, 2019. **10**(1): p. 1-19.
64. Sohail, M., et al., Synthesis of well-dispersed TiO_2@reduced graphene oxide (rGO) nanocomposites and their photocatalytic properties. Materials Research Bulletin, 2017. **90**(1): p. 1-13.
65. Garg, R., N.K. Dutta, and N.R. Choudhury, Work Function Engineering of Graphene. Nanomaterials (Basel), 2014. **4**(2): p. 1-30.
66. Yildirim, O.A. and T. Ozturk, Graphene-Semiconductor Composites as Visible Light-Induced Photocatalyst. 2018. **1**(1): p. 1-12.
67. Khan, M., Graphene based metal and metal oxide nanocomposites: synthesis, properties and their applications. Journal of Materials Chemistry A, 2015. **3**(37): p. 1-18.
68. Azadmanjiri, J., Graphene-supported 2D transition metal oxide heterostructures. Journal of Materials Chemistry A, 2018. **6**(28): p. 1-13.

69. Yang, X. and D. Wang, Photocatalysis: From Fundamental Principles to Materials and Applications. ACS Applied Energy Materials, 2018. **1**(12): p. 1-16.
70. Younis, S. and K.-H. Kim, Heterogeneous Photocatalysis Scalability for Environmental Remediation: Opportunities and Challenges. Catalysts, 2020. **10**(10): p. 1-19.
71. Wang, B., Application of Heterogeneous Catalytic Ozonation for Refractory Organics in Wastewater. Catalysts, 2019. **9**(3): p. 1-14.
72. Yahya, N., A review of integrated photocatalyst adsorbents for wastewater treatment. Journal of Environmental Chemical Engineering, 2018. **6**(6): p. 1-40.
73. Giovannetti, R., Recent Advances in Graphene Based TiO_2 Nanocomposites ($GTiO_2Ns$) for Photocatalytic Degradation of Synthetic Dyes. Catalysts, 2017. **7**(10): p. 1-25.
74. Mobeen Amanulla, A. and R. Sundaram, Green synthesis of TiO_2 nanoparticles using orange peel extract for antibacterial, cytotoxicity and humidity sensor applications. Materials Today: Proceedings, 2019. **8**(1): p. 1-33.
75. Umekar, M.S., Phytoreduced graphene oxide-titanium dioxide nanocomposites using Moringa oleifera stick extract. Materials Today: Proceedings, 2020. **29**(1): p. 1-24.
76. Habte, A.T. and D.W. Ayele, Synthesis and Characterization of Reduced Graphene Oxide Started from Graphene Oxide Using the Tour Method with Different Parameters. Advances in Materials Science and Engineering, 2019. **1**(1): p. 1-9.
77. Štengl, V., et al., TiO_2-graphene oxide nanocomposite as advanced photocatalytic materials. Chemistry Central Journal, 2013. **7**(1): p. 1-41.
78. Phrompet, C., C. Sriwong, and C. Ruttanapun, Mechanical, dielectric, thermal and antibacterial properties of reduced graphene oxide (rGO)-nanosized C_3AH_6 cement nanocomposites for smart cement-based materials. Composites Part B: Engineering, 2019. **175**(1): p. 1-28.
79. Kumar, A., Effect of the band gap and the defect states present within band gap on the non-linear optical absorption behaviour of yttrium aluminium iron garnets. Optical Materials, 2020. **108**(1): p. 1-16.
80. Alkaykh, S., A. Mbarek, and E.E. Ali-Shattle, Photocatalytic degradation of methylene blue dye in aqueous solution by $MnTiO_3$ nanoparticles under sunlight irradiation. Heliyon, 2020. **6**(4): p. 1-33.

81. Yi, C., The preparation of amorphous TiO_2 doped with cationic S and its application to the degradation of DCFs under visible light irradiation. Sci Total Environ, 2019. **684**(1): p. 1-36.
82. Gupta, B., Role of oxygen functional groups in reduced graphene oxide for lubrication. Sci Rep, 2017. **7**(1): p. 1-30.
83. Chong, S.W., C.W. Lai, and S.B. Abdul Hamid, Green preparation of reduced graphene oxide using a natural reducing agent. Ceramics International, 2015. **41**(8): p. 1-29.
84. Zhang, H., Synthesis and characterization of TiO_2/graphene oxide nanocomposites for photoreduction of heavy metal ions in reverse osmosis concentrate. RSC Advances, 2018. **8**(60): p.1-34.
85. AlShammari, A.S., Synthesis of Titanium Dioxide (TiO_2)/Reduced Graphene Oxide (rGO) thin film composite by spray pyrolysis technique and its physical properties. Materials Science in Semiconductor Processing, 2020. **116**(1): p. 1-40.
86. Jaafar, E., Study on Morphological, Optical and Electrical Properties of Graphene Oxide (GO) and Reduced Graphene Oxide (rGO). Materials Science Forum, 2018. **917**(1): p. 1-16.
87. Khan, I., Heterogeneous photodegradation of industrial dyes: An insight to different mechanisms and rate affecting parameters. Journal of Environmental Chemical Engineering, 2020. **8**(5): p. 1-43.
88. Sathiyan, K., Controllable synthesis of TiO_2 nanoparticles and their photocatalytic activity in dye degradation. Materials Research Bulletin, 2020. **126**(1): p. 1-18.

Research Fund Acknowledgement

This research project is funded by Adama Science and Technology University under the grant number ASTU/SM-R/010/19.